X-16494

~~X-16494~~

c.5

*RAC-10970-1

[redacted]

c 8725

SC-DC-66-1931X

REPORT NO. 10970-1

11 JANUARY 1957

SC-DC-66-1931X

PRELIMINARY BALLISTIC CIRCULAR ERROR PROBABILITY

PHASE I, LOTOP PROJECT

RYAN MODEL 109

Sandia Corporation Purchase Order 51-2116

Prepared By: W. W. Wood
W. W. Wood
Computing Group Engineer

Approved By: R. A. Fuhrman
R. A. Fuhrman, Chief
Technical Section

Prepared By: D. R. Craig
D. R. Craig
Sr. Research Engineer

Approved By: R. R. Schwanhausser
R. R. Schwanhausser
Project Engineer

No. of Pages: 63 62P

No. of Figures: 35 98P

SANDIA SYSTEMATIC DECLASSIFICATION REVIEW
1st Review Date: 3-04-97
Authority: ☐ ADC ☒ ADD
Name: W. Layne
2nd Review Date: 3/10/97
Authority: ADD
Name: P. Craner
Comments: OK for Oppenheimer

SANDIA SYSTEMATIC DECLASSIFICATION REVIEW
DOWNGRADING OR DECLASSIFICATION STAMP

CLASSIFICATION CHANGED TO: U	AUTHORITY: R. B. Craner
Emelda Selph 3/6/97	RECORD ID: 97SN623
PERSON CHANGING MARKING 3/11/97	
Carmela M Gallegos	DATED: 3/10/97
PERSON VERIFYING MARKING & DATE	

INVENTORIED

1957

2743

[redacted]

1600

[redacted]

TABLE OF CONTENTS

Section		Page
1.0	SUMMARY	1.1
2.0	INTRODUCTION	2.1
3.0	METHOD OF APPROACH	3.1
3.1	Launch Trajectory	3.2
3.1.1	Errors Considered	3.2
3.1.2	Plan of Computation	3.2
3.2	Loop Trajectory	3.4
3.2.1	Errors Considered	3.4
3.2.2	Plan of Computation	3.4
4.0	DISCUSSION	4.1
4.1	Launches	4.1
4.1.1	Variations of Thrust Magnitude	4.1
4.1.2	Variations of Thrust Alignment	4.3
4.2	Loop Trajectories	4.4
4.3	Total Ballistic Circular Error	4.5
5.0	CONCLUSIONS	5.1
6.0	APPENDIX	6.1
6.1	References	6.2
6.2	List of Symbols	6.3
6.3	Equations	6.7
6.3.1	Equations Used for Longitudinal Launch Studies - Canard Off	6.7
6.3.2	Equations Used for Lateral Launch Studies - Canard Off	6.8
6.3.3	Autopilot Equations	6.9

INDEX OF FIGURES

Figure		Page
2.1	Typical Mission Profile	2.3
2.2	Ryan Model 109-G	2.4
3.1	General Arrangement of Model 109-G	3.5
4.1	Comparison of Given Burning with Assumed Reference Burning -- F_n vs Time	4.7
4.2	Comparison of Given Burning with Assumed Reference Burning -- h vs x	4.8
4.3	Comparison of Given Burning with Assumed Reference Burning -- V_T vs Time	4.9
4.4	Comparison of Given Burning with Assumed Reference Burning -- $\dot{V}_T$ vs Time	4.10
4.5	Comparison of Given Burning with Assumed Reference Burning -- α vs Time	4.11
4.6	Comparison of Given Burning with Assumed Reference Burning -- $\dot{\theta}$ vs Time	4.12
4.7	Comparison of Given Burning with Assumed Reference Burning -- $\bar{\theta}$ vs Time	4.13
4.8	Comparison of Random Burning with Assumed Reference Burning -- F_n vs Time	4.14
4.9	Comparison of Random Burning with Assumed Reference Burning -- h vs x	4.15
4.10	Comparison of Random Burning with Assumed Reference Burning -- V_T vs Time	4.16
4.11	Comparison of Random Burning with Assumed Reference Burning -- $\dot{V}_T$ vs Time	4.17
4.12	Comparison of Random Burning with Assumed Reference Burning -- α vs Time	4.18
4.13	Comparison of Random Burning with Assumed Reference Burning -- $\dot{\theta}$ vs Time	4.19

Figure		Page
4.14	Comparison of Random Burning with Assumed Reference Burning -- $\ddot{\theta}$ vs Time	4.20
4.15	Comparison of Three Types of Days -- h vs x	4.21
4.16	Comparison of Three Types of Days -- V_T vs Time	4.22
4.17	Comparison of Three Types of Days -- $\dot{V}_T$ vs Time	4.23
4.18	Comparison of Three Types of Days -- α vs Time	4.24
4.19	Comparison of Three Types of Days -- $\dot{\theta}$ vs Time	4.25
4.20	Comparison of Three Types of Days -- $\ddot{\theta}$ vs Time	4.26
4.21	Comparison of Three Vertical Thrust Line Locations h vs x	4.27
4.22	Comparison of Three Vertical Thrust Line Locations V_T vs Time	4.28
4.23	Comparison of Three Vertical Thrust Line Locations $\dot{V}_T$ vs Time	4.29
4.24	Comparison of Three Vertical Thrust Line Locations α vs Time	4.30
4.25	Comparison of Three Vertical Thrust Line Locations $\dot{\theta}$ vs Time	4.31
4.26	Comparison of Three Vertical Thrust Line Locations $\ddot{\theta}$ vs Time	4.32
4.27	Comparison of Three Lateral Thrust Line Locations y vs x	4.33
4.28	Comparison of Three Lateral Thrust Line Locations $\dot{V}$ vs Time	4.34
4.29	Comparison of Three Lateral Thrust Line Locations $\dot{\phi}$ vs Time	4.35
4.30	Comparison of Three Lateral Thrust Line Locations $\ddot{\phi}$ vs Time	4.36
4.31	Comparison of Three Lateral Thrust Line Locations $\dot{\psi}$ vs Time	4.37
4.32	Comparison of Three Lateral Thrust Line Locations $\ddot{\psi}$ vs Time	4.38

1.0 SUMMARY

As a part of Phase I of the LOTOP Project, both analog and digital computations were made to determine the ballistic accuracy of the Ryan Model 109-G. The scope of the study was limited by the change of emphasis indicated in References 3 through 5. Completion of the Circular Error Probability (CEP) studies is planned during the extension of Phase I (Reference 2). The basic assumptions for the present studies included perfect release conditions and an ideal environment. The planned extension of the studies will cover operational errors resulting in imperfect launches as well as such factors as surface winds and turbulence.

The Phase I studies were divided into two parts. The first investigated dispersion during launch while the rockets are burning; the second, variations in the loop trajectory. Source errors considered were (a) variations in the magnitude and direction of the thrust vector during launch and (b) structural asymmetries. Their various effects were studied independently. Both digital and analog computations were made.

Subject to the limiting assumptions, it was found that ballistically the Ryan Model 109-G can repeat trajectories with considerable precision. Variations in rate of burning have practically no effect, provided total impulse remains constant. Variations in rocket alignment of 1/2 inch above and below the store c.g. indicated no effect on horizontal distance traveled and showed vertical variations of only 8 to 11 feet at pull-up. The structural imperfection affecting the trajectory most significantly was wing twist, where 1/2° of twist resulted in a terminal point variation of 165 feet. Manufacturing tolerances of 1/2° of twist or less may easily be maintained for the 109-G. The

studies to date show that for a given error source the maximum radial displacement of the terminal point of the loop is less than 200 feet, whereas the specified requirement is that the median radial error have a value not greater than 500 feet.

2.0 INTRODUCTION

The Ryan Aeronautical Company has received a contract from the Sandia Corporation (Purchase Order 51-2116) for the Phase I design study of a low-altitude external store delivery system assigned the unclassified title "LOTOP". The store is to be launched from a fighter or attack type aircraft after which it is to perform a loop-type maneuver for delivery of the payload to the target. (See Figure 2.1).

A low delta wing configuration with canard control surfaces has been developed which is designated the Ryan Model 109-G (Figure 2.2). The purpose of this report is to present the results of a study performed to evaluate the ballistic accuracy of the Model 109-G. It is necessary to show that, given identical conditions of release and environment, trajectories can be consistently repeated which satisfy the criteria established for the Circular Error Probability (CEP).

The Phase I ballistic CEP requirements demand a delivery system which, under like release conditions, allows for at least 50 percent of the terminal trajectories to pass completely within a cylinder of 500 feet radius centered at the target and extending 3000 feet above the launch altitude. Figure 2.1 shows the ballistic CEP requirements in relation to the total maneuver as well as the operational CEP requirements which will be used in the extension of these studies. The extended studies will not assume perfect release but will cover the effects of operational and environmental errors on the repeatability of trajectories (Reference 2).

References 3 through 5 dictated the magnitude of the CEP studies reported herein. Computations were performed at Ryan on a PACE analog computer and on an IBM Type 650 digital computer. The effects of source errors were considered separately. In the anticipated extension of these studies it is planned to study the possible ways in which various source errors may combine.

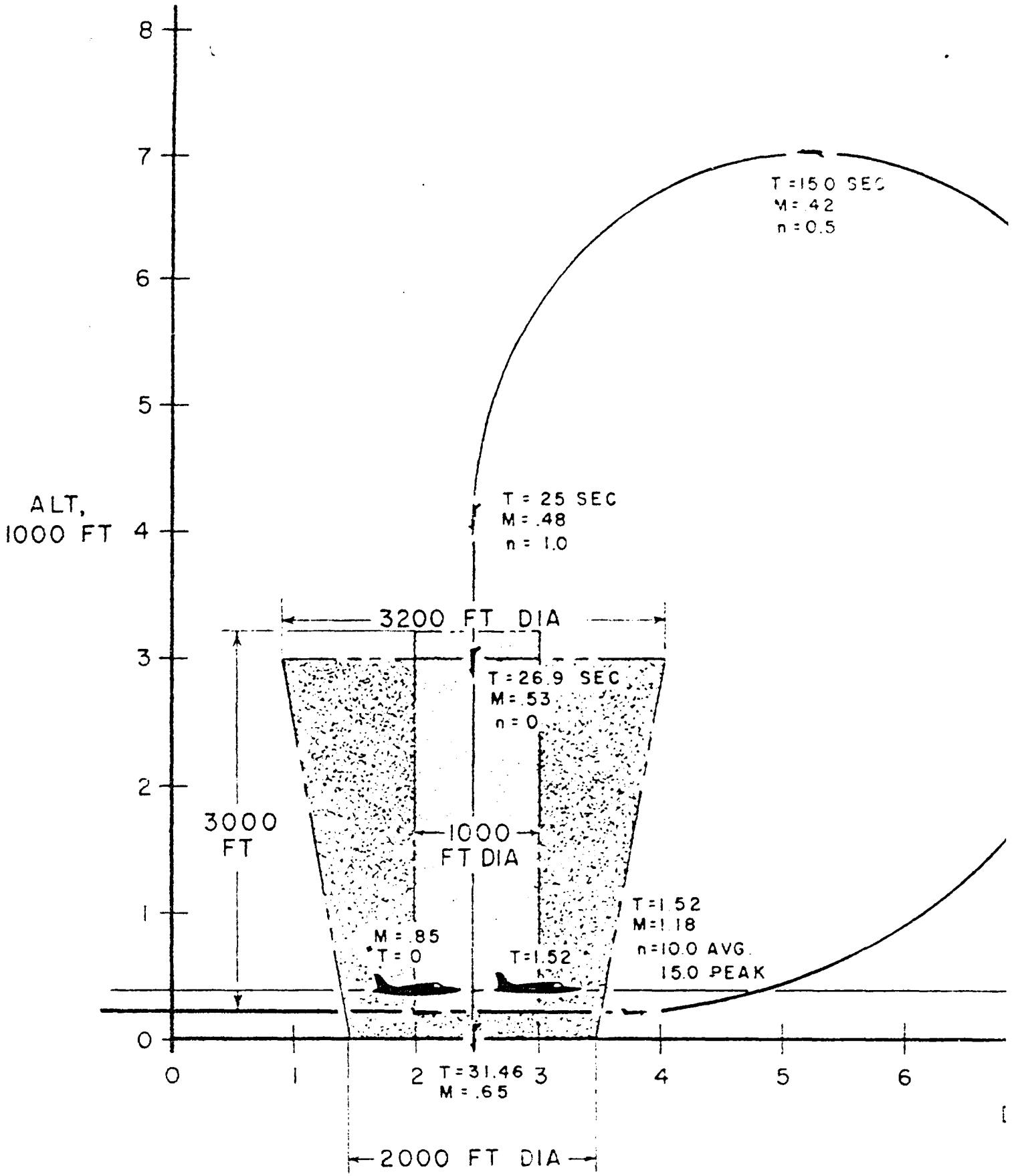

*T = TIME FROM LAUNCH POINT

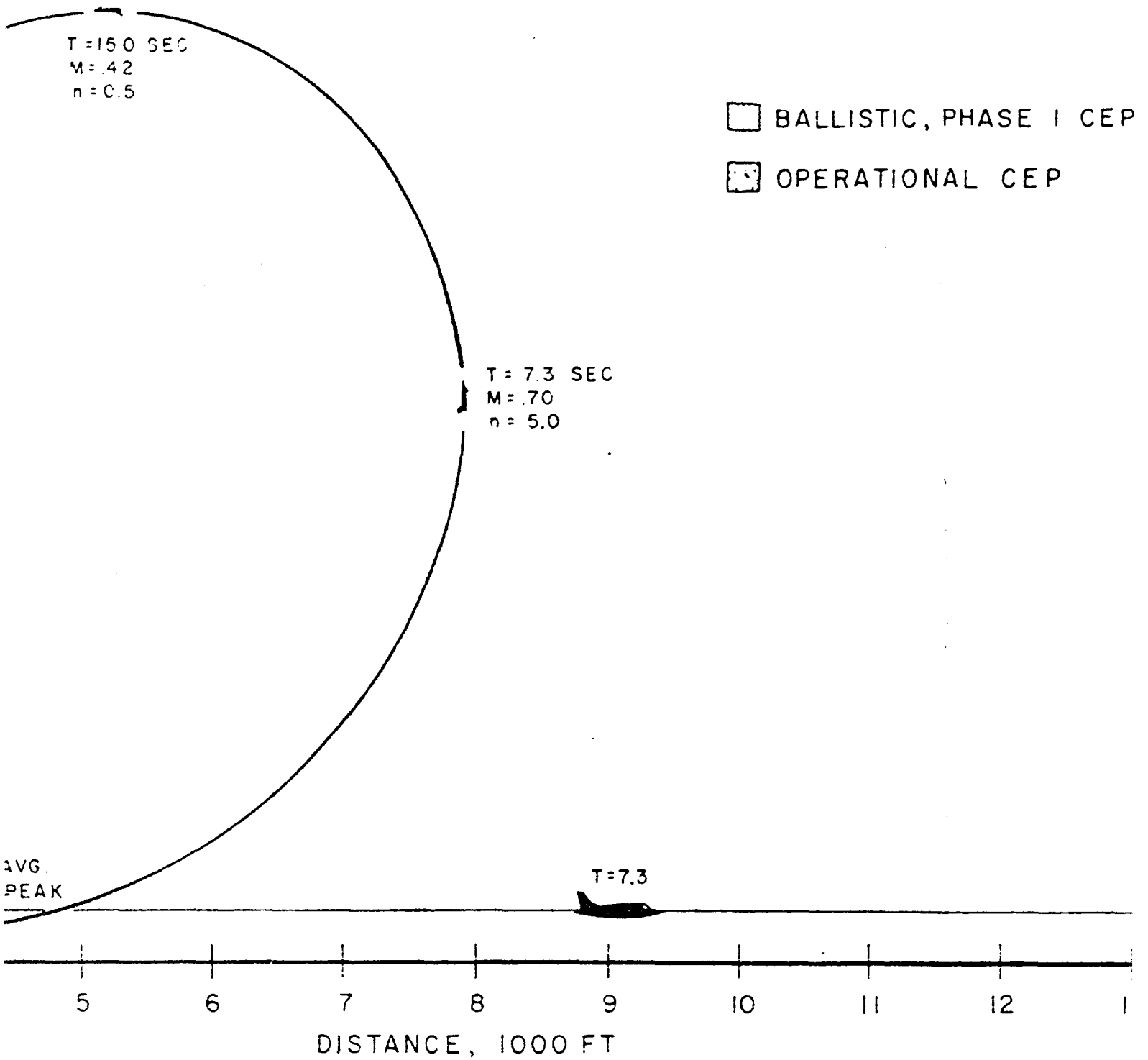

MODEL 109G TYPICAL MIS

Figure 2.1

BALLISTIC, PHASE I CEP

OPERATIONAL CEP

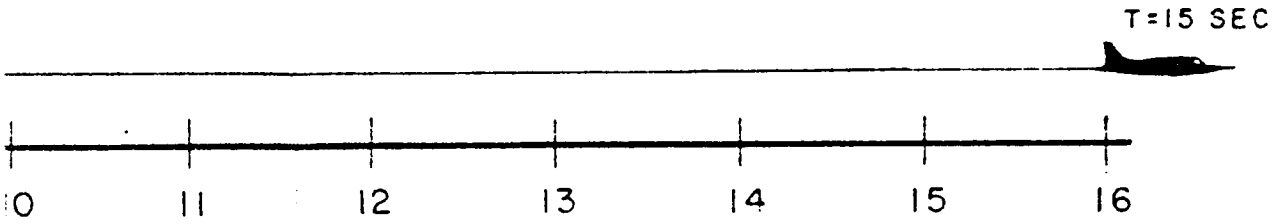

109G TYPICAL MISSION PROFILE

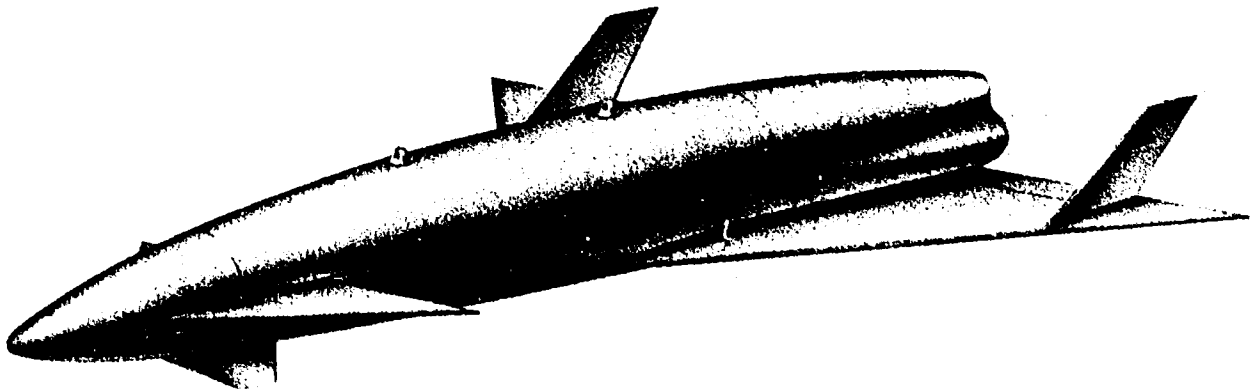

RYAN MODEL 109-G

Figure 2.2

3.0 METHOD OF APPROACH

The Phase I CEP studies were limited in accordance with References 3, 4 and 5. Therefore, it was not considered practical to do a complete probability analysis. Instead individual errors were examined in order to qualitatively evaluate the probable ballistic error. In the extended CEP studies, Reference 2 , a quantitative probability analysis will be made of the operational CEP.

Since the Model 109-G is provided with power for separation, it was convenient for these studies to divide the mission into two parts. The first part of the mission is the launch period when the rockets are burning. The second part is the unpowered portion during which a pull-up is commanded and the store describes a loop-type trajectory. The study was primarily concerned with the vehicle's inherent ballistic characteristics. Therefore the assumptions of control characteristics were kept as simple as possible. The studies in the pitching plane assumed either retracted or fixed canard deflection, and for the lateral studies relatively simple equations for the vertical canard surface and aileron motions were introduced.

Directly after release the vehicle undergoes a rapid acceleration and, at the time the rockets are burning out, the thrust falls to zero abruptly. Because forces are changing rapidly, great accuracy is required for this stage of the computations. It was decided to perform all the launch studies on the digital computer, the IBM Type 650. The loop trajectories, on the other hand, are somewhat less sensitive and they were calculated on the "PACE" analog computer. This seemed justified since previous analog loop trajectories had shown good agreement with those performed on the digital computer.

Figure 3.1 presents a three-view drawing of the Model 109-G.

3.1 Launch Trajectory

Perfect release conditions were assumed in all cases. This included an assumption of perfect store alignment on the launch aircraft. A further simplification was made to ignore independent action of the three rockets and to describe the resultant thrust vector as if it were from a single origin. In keeping with the philosophy of minimal restrictions with regard to automatic control, the longitudinal studies disregarded movement of the canard surfaces. The lateral cases, while "driven" from information developed during the longitudinal studies, assumed control of ailerons and vertical canard surface. The control equations used are presented in the Appendix to this report.

3.1.1 Errors Considered

The launch studies investigated dispersion and the development of forces and moments that might adversely affect the pull-up. All these quantities were assumed to be functions of the thrust vector, variations of which in magnitude or alignment were used as source errors.

3.1.2 Plan of Computation

In order to study the launch as thoroughly as possible and with a minimum of linearization, it was decided to conduct longitudinal and lateral computations separately, using virtually the full capacity of the Type 650 for each set of computations. The longitudinal calculations were made first, and they investigated the effect of variations of the thrust vector both with respect to magnitude and alignment.

In studying changes in thrust magnitude, three possible sources of error were considered. First, cases were run to check the validity of the straight-line approximations of the thrust curves. Throughout the previous Model 109-G trajectory studies, each of the thrust curves given in Reference 6 was approximated by three straight lines. For purposes of the present studies, the effects of these approximations were compared with results derived from carefully fitting the given curves. Second, recognizing that the burning of a rocket may be somewhat uneven, random variations in thrust magnitude were introduced. This was done by estimating the greatest random change likely to occur within a given time increment, assigning to this value a probability of .09, and introducing random errors in accordance with a normal distribution. Each error was added to the preceding value of thrust, so that the total error could randomly accumulate or cancel out. Third, the effect of grain temperature or burning rate was considered.

Longitudinal studies were conducted to show the effect of vertical misalignment of the thrust vector. It was assumed that the vector remained parallel to the ideal position but might be as much as half an inch above or below the vehicle's center of gravity.

Studies were also made of lateral misalignment. These were "driven" from the computations made for the vertical cases, but angular error as well as vertical and lateral offsets was introduced. The reason for considering angular error was that it allowed the possibility of developing rolling moment and roll angle. Though dependent on the separately performed longitudinal computations, the results of the lateral computations are considered reasonably accurate within the limitations of this program. The lateral equations of motion are shown in the Appendix.

3.2 Loop Trajectory

Loop trajectories were calculated on a "PACE" analog computer in connection with studies for the Model 100-G control system reported in Reference 7. These trajectories were also planned to provide information concerning the ballistic CEP.

3.2.1 Errors Considered

Displacement at the terminal point of the loop was the final result desired. The source errors thought to be most important were structural asymmetries such as wing twist or fin twist, and lateral deviations at the time of pull-up; i.e., the presence of non-zero roll angle, yaw angle, or side velocity.

3.2.2 Plan of Computation

The analog set-up is described in Reference 7 . It will be noted that, consistent with small perturbation theory, many of the aerodynamic derivatives were held constant. The autopilot equations, on the other hand, included considerations of time lag.

4.0 DISCUSSION

In the preliminary ballistic CEP study no attempt was made to determine the probable distribution of errors. Rather, the object was to consider independently the maximum errors likely to arise from variations in rocket performance or from structural imperfections.

4.1 Launches

The results of the launch studies are presented graphically in Figures 4.1 through 4.32.

The end point of a launch is considered to be that point at which pull-up is commanded. Although the distance traveled before rocket burn-out may vary considerably, it has been assumed for this study that the end point of the launch is that time at which the vehicle is 300 feet ahead of the launch airplane. Normally rocket burn-out occurs before the end of the launch phase.

4.1.1 Variations of Thrust Magnitude

The basic data on rocket thrust were taken from Reference 6. However, throughout the studies of the Model 100-G, it was convenient to approximate the given thrust curves by three straight lines. Figure 4.1 shows the given thrust curves and their straight line approximations. All comparisons of thrust have been referred to the approximation used for a standard day. This has been described as the "Assumed Reference Burning". On many of the graphs this is indicated by the abbreviation REF. In Figure 4.1, the word "given" is used to designate the curves given in the manufacturer's specification (Reference 6).

Figures 4.2 through 4.7 demonstrate that the three straight lines are in fact a very good approximation. The actual acceleration along the flight path closely follows the input thrust, as shown in Figure 4.4. These curves show approximately the same difference as the thrust curves in Figure 4.1. The variables shown in Figure 4.3 and 4.5 through 4.7 are almost unaffected except that in all cases the approximated thrust showed an earlier burn-out time. Otherwise, even the timing is virtually identical, as shown in Figure 4.2. This figure includes the flight path of the launch airplane. There is no measurable difference between the flight paths computed from the given curves, and those computed from the straight line approximations. The time arrows show that on either of any pair of flight paths the same position is reached at the same time. However, the flight paths computed from the given thrust curves show that at the time the vehicle has reached a point 300 feet in front of the launch airplane final burn-out has not yet occurred.

Since rockets display considerable unevenness in burning, a study was made to evaluate this as a source of dispersion. Five cases were run in which a random variation of thrust was introduced during the period normally considered to have constant thrust. It is seen in Figure 4.8 that the deviations are completely irregular, and the departure from the assumed reference in one case exceeded 500 pounds. The effect of these random variations on the motion of the vehicle, however, was negligible. It is evident from Figures 4.9 through 4.14 that irregularities of burn rate present no difficulty.

On a hot day the rockets may be expected to burn faster than on a cold day. This results in greater thrust applied over a shorter period of time.

The total impulse, however, remains approximately the same. Although the differences in acceleration affect the vehicle's flight path, the distances involved are small. Thus, as seen in Figure 4.15, the greatest horizontal displacement from standard day conditions is 140 feet, and the greatest vertical displacement is 20 feet. These values are well within the allowed tolerances and might be considered predictable differences in performance rather than errors. Acceleration along the flight path (Figure 4.17) reflects the assumed thrust, and the velocity graph (Figure 4.16) indicates slower build-up on cold days with a maximum difference in final velocity of 130 feet per second. Angular motions in the pitching plane (see Figures 4.18 through 4.20) damp out rapidly, especially at the higher Mach numbers.

4.1.2 Variations of Thrust Alignment

The first cases of thrust misalignment assumed that the thrust vector remained parallel to the ideal position, but was vertically offset from the center of gravity by half an inch. This, obviously, is a source of vertical dispersion, but the maximum displacement is only ten feet. In Figure 4.21, $e = 0.5$ indicates that the thrust line is 1/2 inch below the c.g. and $e = -0.5$ indicates that the thrust line is 1/2 inch above the c.g. The offset affects velocity and acceleration so little that the differences cannot be plotted. See Figures 4.22 and 4.23. With regard to angle of attack and pitching rate and acceleration (Figures 4.24 through 4.26), it is seen that there is a phase angle of roughly 180° between the plus and minus cases. The zero case lags behind the minus case by about 30°, but with much smaller amplitudes. All these angular quantities damp rapidly, especially at the higher Mach numbers. So far as the pitch angle itself

is concerned, the offset has little effect. At end of launch the pitch angle varied from -1.9° for $e = 0.5$ at $M = .95$ to -3.6° for $e = -0.5$ at $M = .70$.

The results of these misalignment computations in the pitching plane were used to "drive" further computations exploring the effects of lateral misalignments. A lateral offset, $\bar{e} = 0.5$ in., was added, as well as an angular incidence, $i_{F_n} = -1^{\circ}$, representing an angle between the thrust vector and the x-y plane of the vehicle's body axis.

Figures 4.27 through 4.32 show that nowhere do the vertical components of offset have a significant effect. Figure 4.28 shows that side acceleration damps slowly, and the same is true of roll and yaw rates and accelerations (Figures 4.29 through 4.32). However, the actual displacements never become large. Thus, in Figure 4.27 it is seen that the lateral displacements at end of launch range from about 5 feet for initial $M = .95$ to 7 feet for $M = .70$. Terminal side velocity never exceeded 6 feet per second. The greatest roll angle developed at any time during the launch was 2.3°; the greatest yaw angle, 1.5°. At the end of launch these had been reduced, however, so that the maximum angular errors were all under $.2^{\circ}$.

4.2 Loop Trajectories

It was considered that the most important ballistic deviation during the loop maneuver would result from lateral deviations due to structural asymmetries or adverse conditions at the time pull-up is commanded. Table 4.1 shows, for various source-errors, the lateral displacement (absolute value) in feet, at the completion of the loop.

Table 4.1

LATERAL DISPLACEMENT AT TERMINATION POINT (FEET)

Source Error	q_o in lbs ft^2 1200	1500	2000	2500
$1/2^\circ$ wing twist	165	90	105	100
$1/2^\circ$ fin twist	100	35	10	50
$\varphi = 5^\circ$ at pull-up	55	55	57	58
$\psi = 2^\circ$ at pull-up	160	150	140	140
v = 20 ft sec at pull-up	105	100	90	85
	278	212	205	205

Note: This is essentially the same as Table 4.6, Reference 7.

The assumed source errors are greater than those actually expected. Even with the above assumptions the maximum displacement for a single source error is only 165 feet.

4.3 Total Ballistic Circular Error

The input values for roll angle and yaw angle used in obtaining the results in Table 4.1 were far in excess of any of the values obtained from the launch computations. Furthermore, the side velocity assumed was 20 feet per second, whereas launch studies indicated that the side velocity at time of pull-up would never be greater than about 6 feet per second. It may, therefore, be assumed that the displacements shown in the last three rows of Table 4.1 are in excess of those to be expected if less conservative values had been used.

The largest deviation encountered in the launch studies was a difference of 14.0 feet in longitudinal position of the end-point, depending on temperature. As indicated before, this type error is predictable and should not be considered a ballistic error. The largest lateral deviation during launch was 7 feet. Added as a positional error to any of the separate lateral displacements shown in Table 4.1, the total error is still well under 200 feet. The exact manner in which these various source errors may combine to affect the ballistic CEP will be examined as a part of the extended Phase I studies.

Figure 4.1

MODEL 109-G CANARD OFF

COMPARISON OF GIVEN BURNING WITH ASSUMED REFERENCE BURNING -- F_n vs TIME

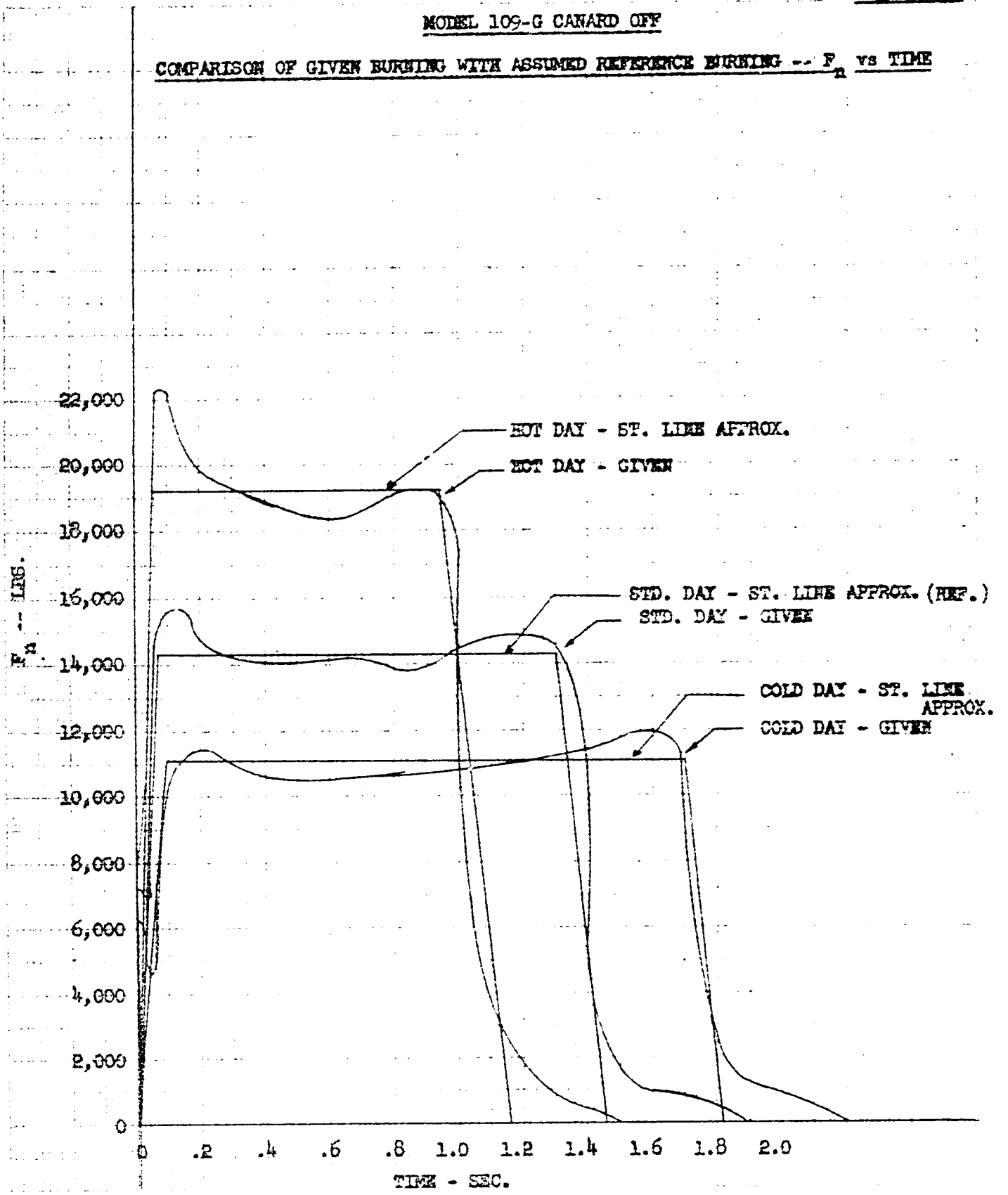

Figure 4.2

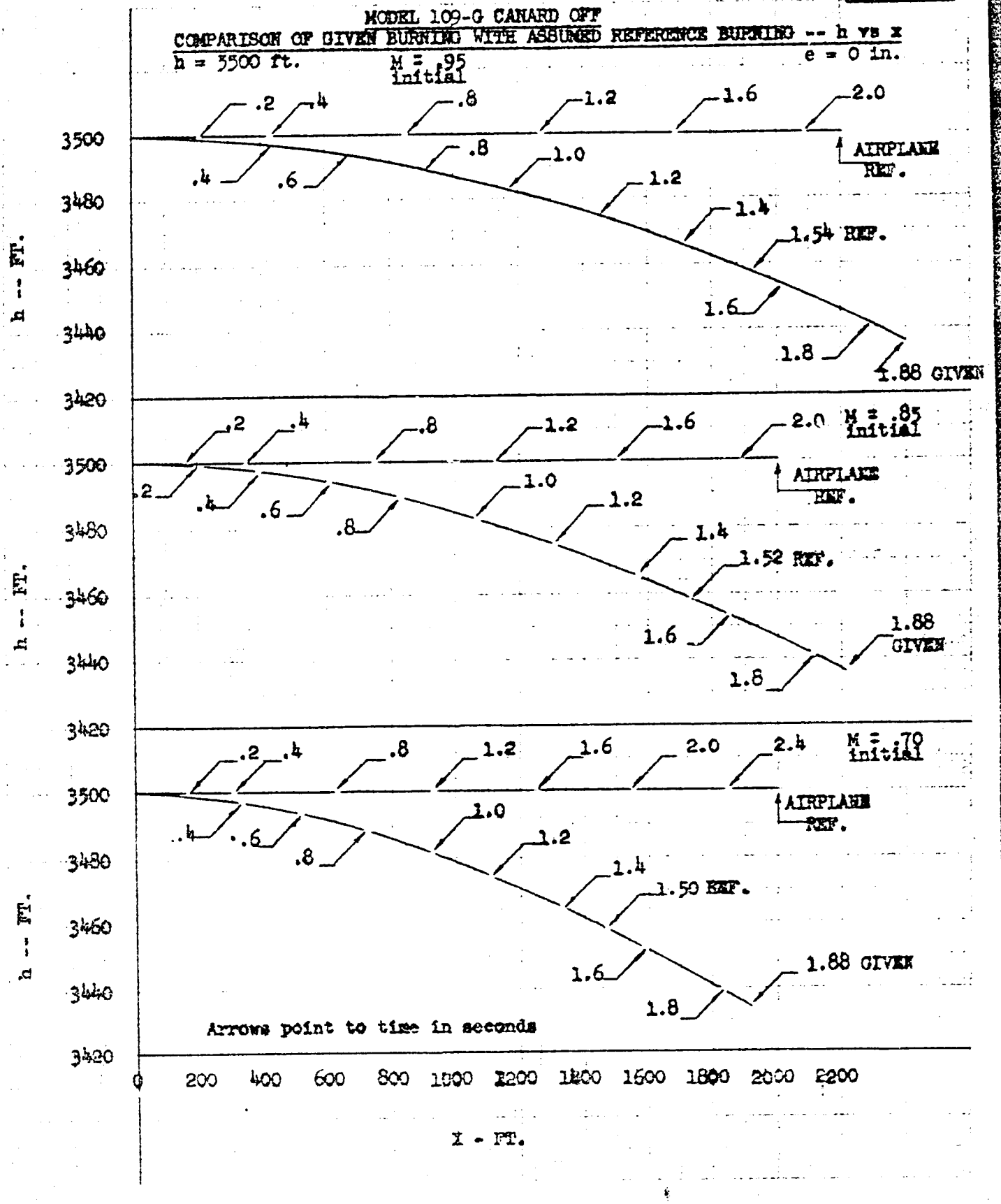
MODEL 109-G CANARD OFF
COMPARISON OF GIVEN BURNING WITH ASSUMED REFERENCE BURNING -- h vs x
h = 3500 ft.
M = .95 initial
e = 0 in.
.2
.4
.8
1.2
1.6
2.0
AIRPLANE REF.
.4
.6
.8
1.0
1.2
1.4
1.54 REF.
1.6
1.8
1.88 GIVEN
M = .85 initial
.2
.4
.6
.8
1.0
1.2
1.4
1.52 REF.
1.6
1.8
1.88 GIVEN
M = .70 initial
2.4
1.50 REF.
Arrows point to time in seconds
h -- FT.
3500
3480
3460
3440
3420
0
200
400
600
800
1000
1200
1400
1600
1800
2000
2200
X - FT.

Figure 4.3

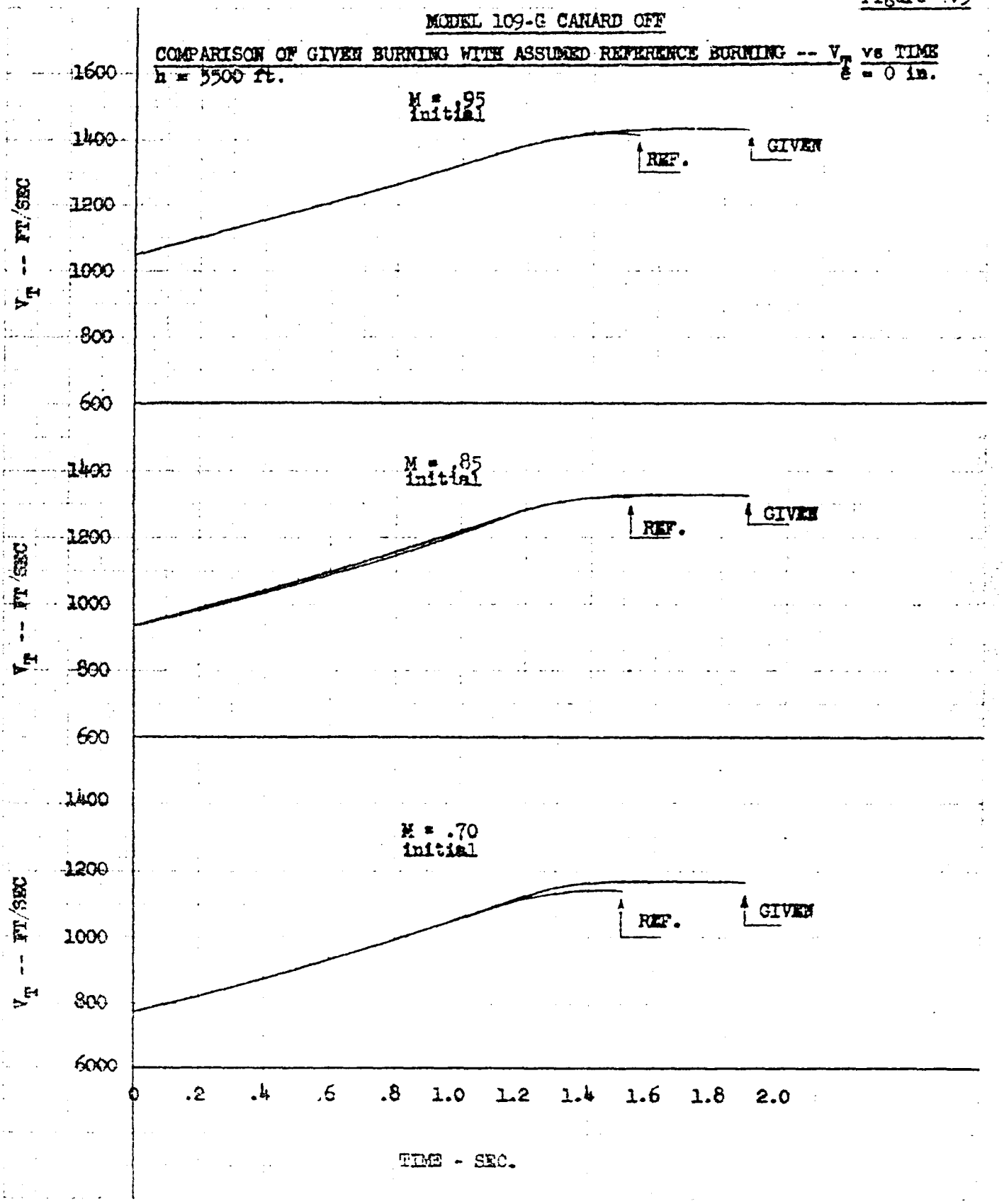
MODEL 109-G CANARD OFF
COMPARISON OF GIVEN BURNING WITH ASSUMED REFERENCE BURNING -- V_T vs TIME
h = 5500 ft.
ε = 0 in.
M = .95 initial
M = .85 initial
M = .70 initial
REF.
GIVEN
V_T -- FT/SEC
1600
1400
1200
1000
800
600
6000
0
.2
.4
.6
.8
1.0
1.2
1.4
1.6
1.8
2.0
TIME - SEC.

Figure 4.4

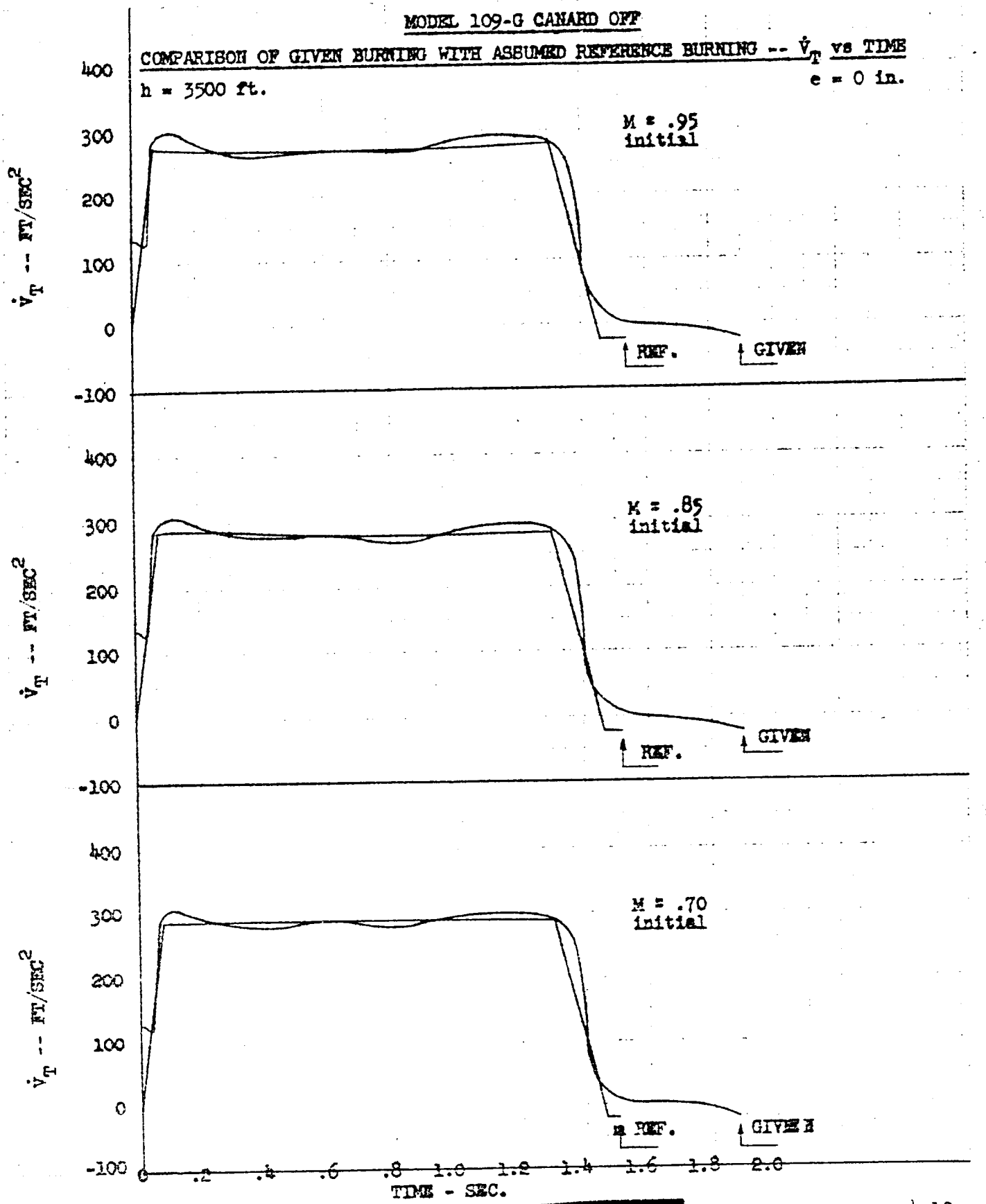
MODEL 109-G CANARD OFF
COMPARISON OF GIVEN BURNING WITH ASSUMED REFERENCE BURNING -- $\dot{V}_T$ vs TIME
h = 3500 ft.
e = 0 in.
M = .95 initial
M = .85 initial
M = .70 initial
REF.
GIVEN
$\dot{V}_T$ -- FT/SEC^2
400
300
200
100
0
-100
0
.2
.4
.6
.8
1.0
1.2
1.4
1.6
1.8
2.0
TIME - SEC.

Figure 4.5

MODEL 109-G CANARD OFF

COMPARISON OF GIVEN BURNING WITH ASSUMED REFERENCE BURNING -- α vs TIME

h = 3500 ft. e = 0 in.

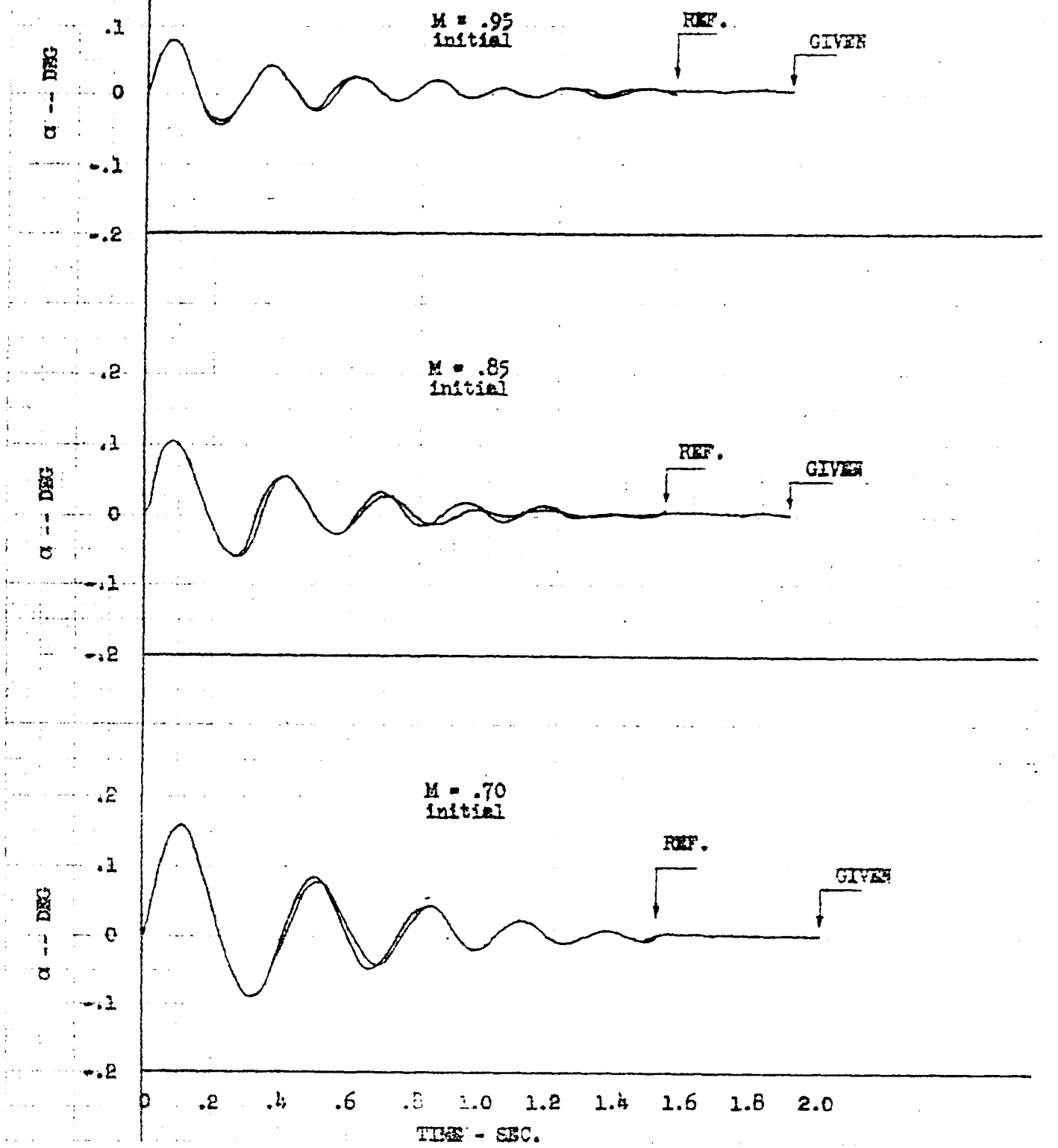

Figure 4.6

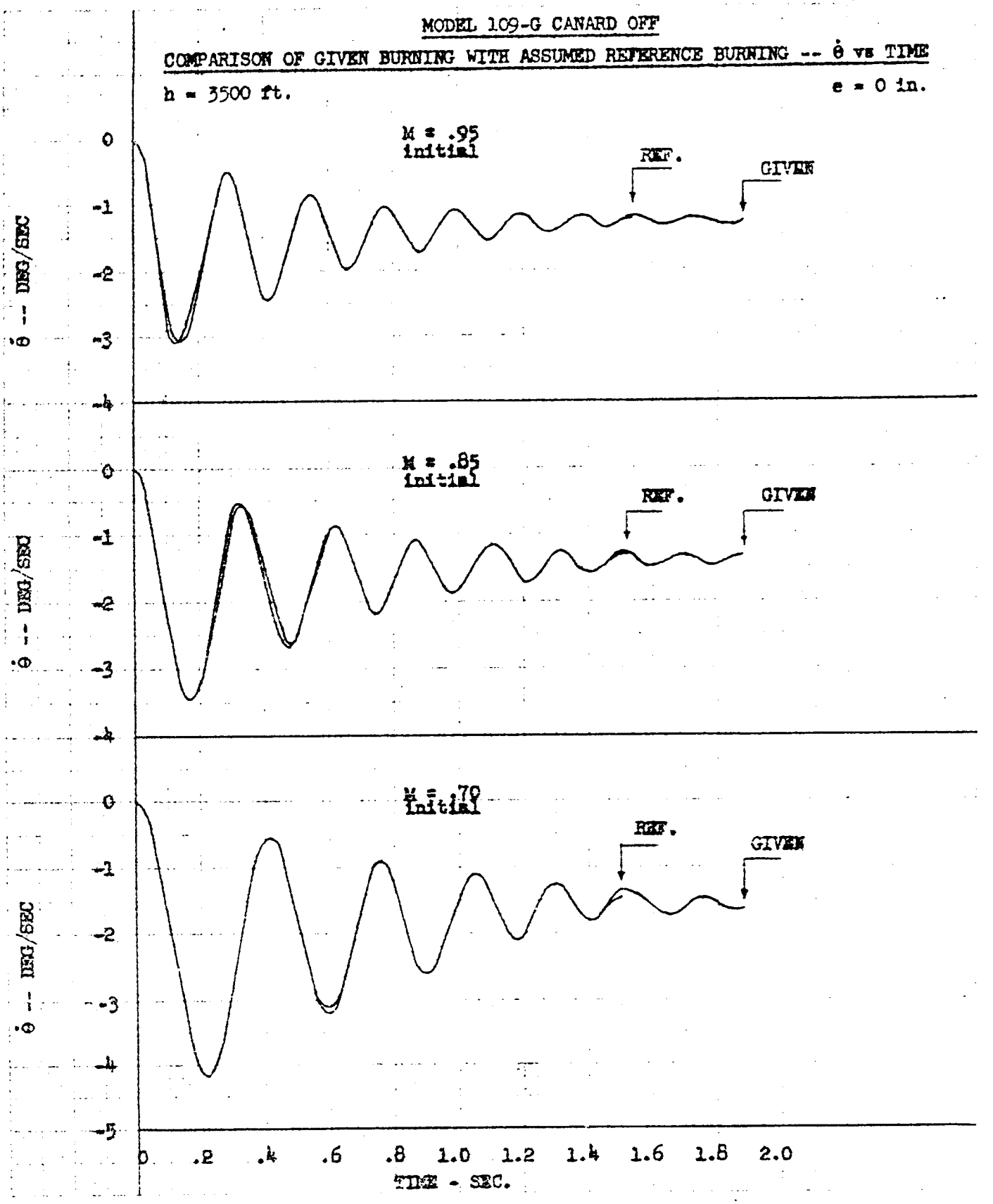
MODEL 109-G CANARD OFF
COMPARISON OF GIVEN BURNING WITH ASSUMED REFERENCE BURNING -- θ̇ vs TIME
h = 3500 ft.
e = 0 in.
M = .95
initial
REF.
GIVEN
M = .85
initial
REF.
GIVEN
M = .70
initial
REF.
GIVEN
θ̇ -- DEG/SEC
0
-1
-2
-3
-4
-5
0
.2
.4
.6
.8
1.0
1.2
1.4
1.6
1.8
2.0
TIME - SEC.

Figure 4.7

MODEL 109-G CANARD OFF

COMPARISON OF GIVEN BURNING WITH ASSUMED REFERENCE BURNING -- $\ddot{\theta}$ vs TIME

h = 3500 ft. e = 0 in.

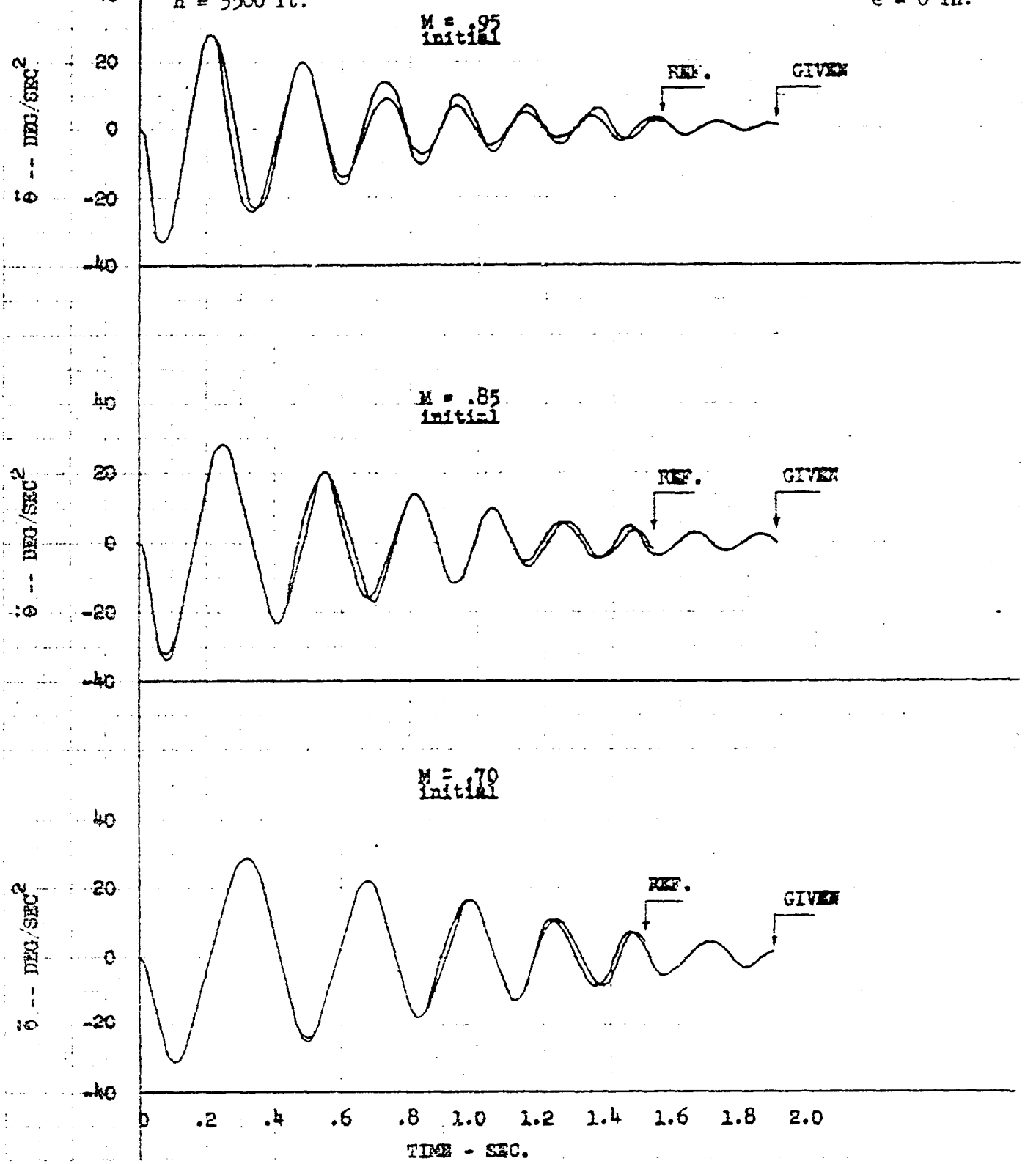

Figure 4.8

MODEL 109-G CANARD OFF

COMPARISON OF RANDOM BURNING WITH ASSUMED REFERENCE BURNING -- F_n vs TIME

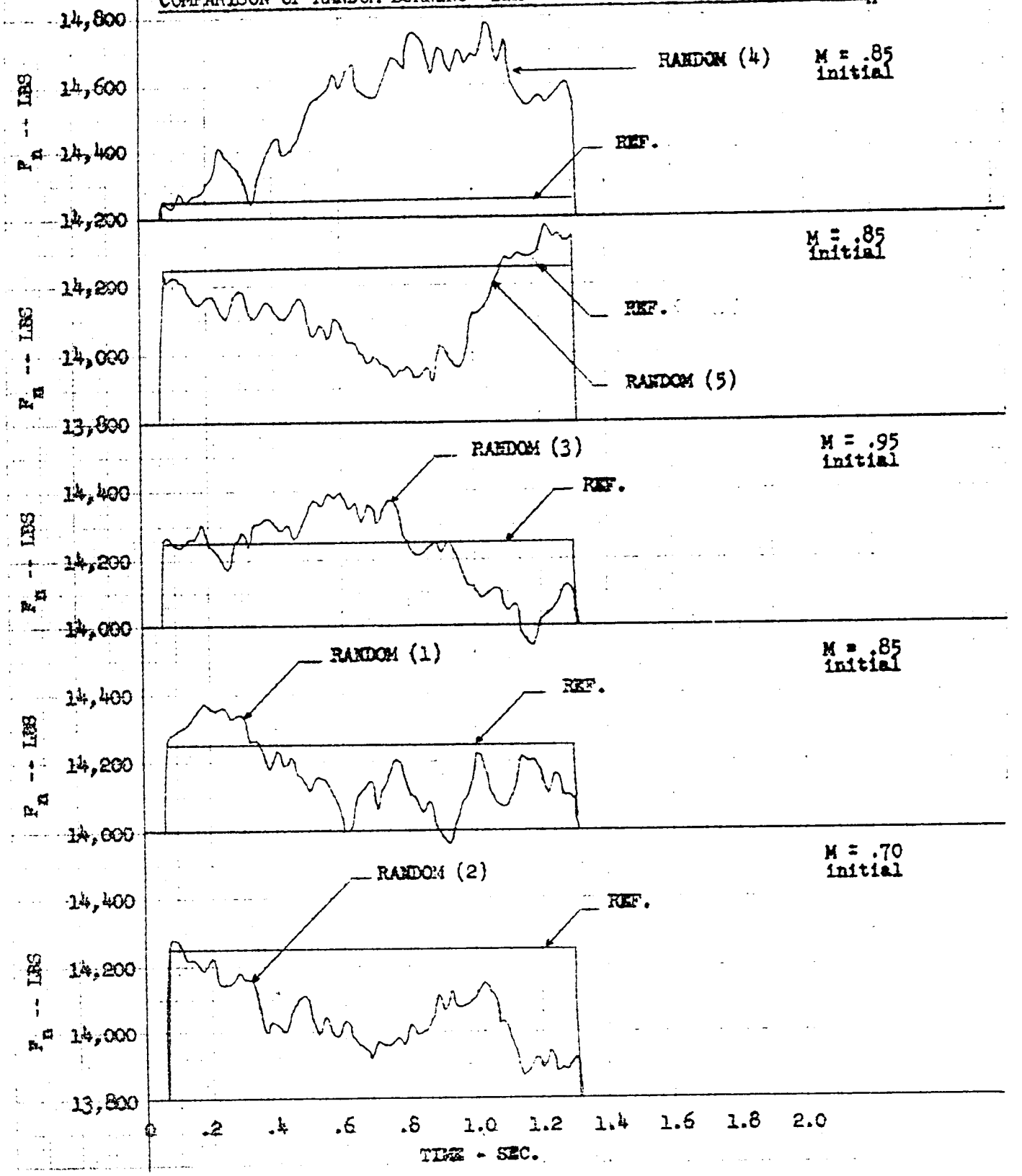

Figure 4.9

MODEL 109-G CANARD OFF

COMPARISON OF RANDOM BURNING WITH ASSUMED REFERENCE BURNING -- h vs x

h = 3500 ft. M = .95 initial e = 0 in.

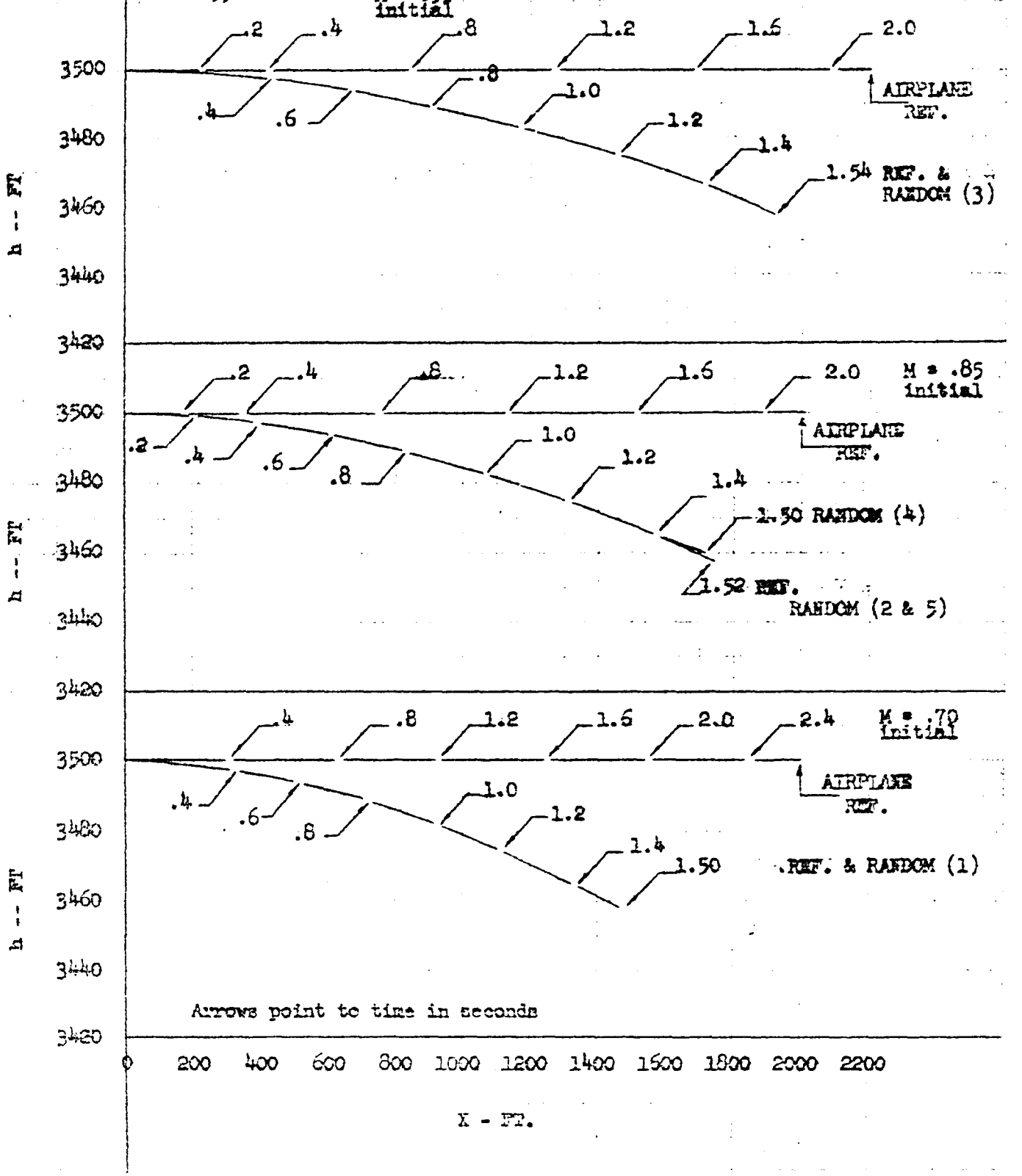

Figure 4.10

MODEL 109-G CANARD OFF

COMPARISON OF RANDOM BURNING WITH ASSUMED REFERENCE BURNING -- V_T vs TIME

h = 3500 ft. e = 0 in.

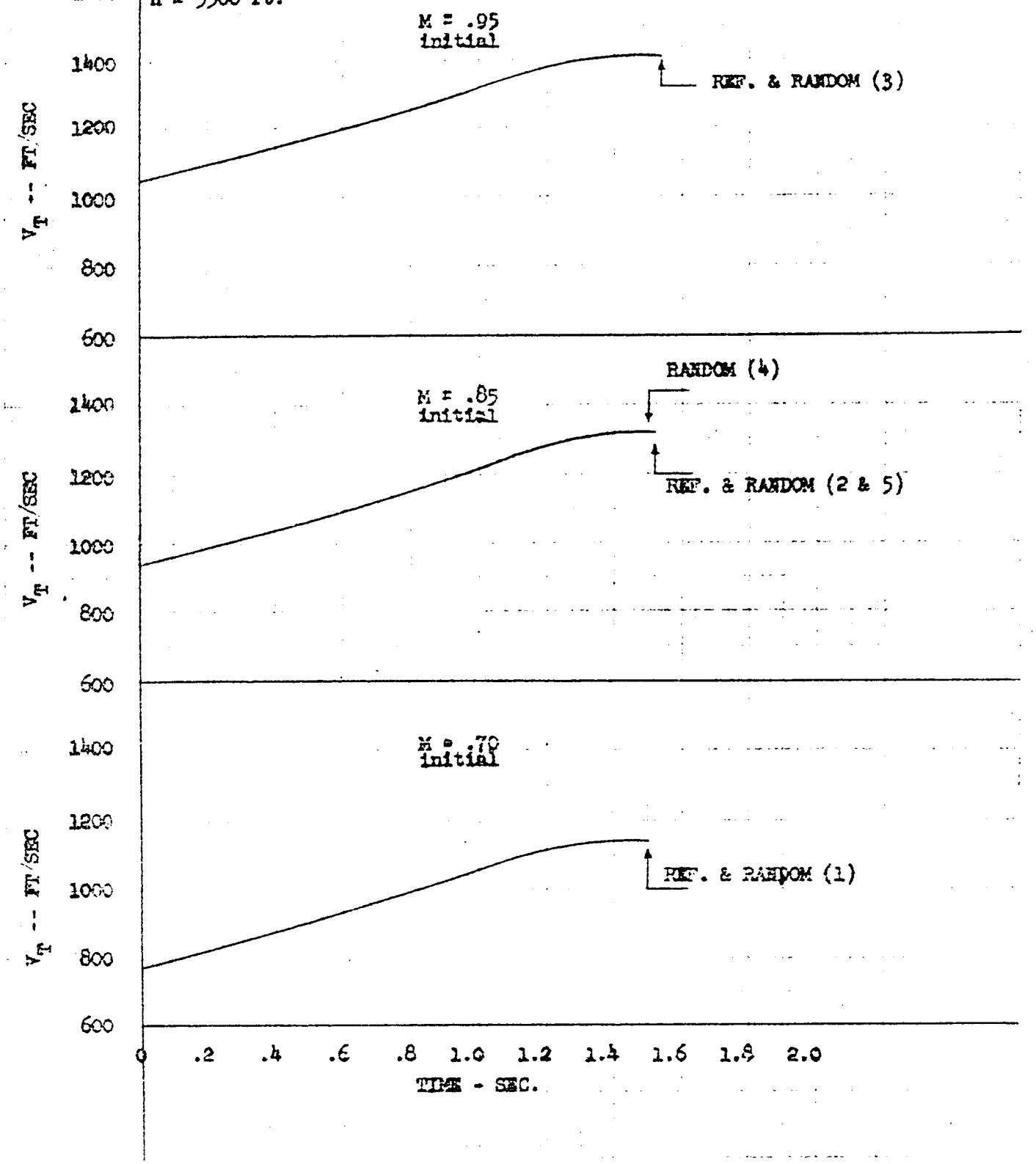

Figure 4.11

MODEL 109-G CANARD OFF

COMPARISON OF RANDOM BURNING WITH ASSUMED REFERENCE BURNING -- $\dot{V}_T$ vs TIME

h = 3500 ft.

e = 0 in.

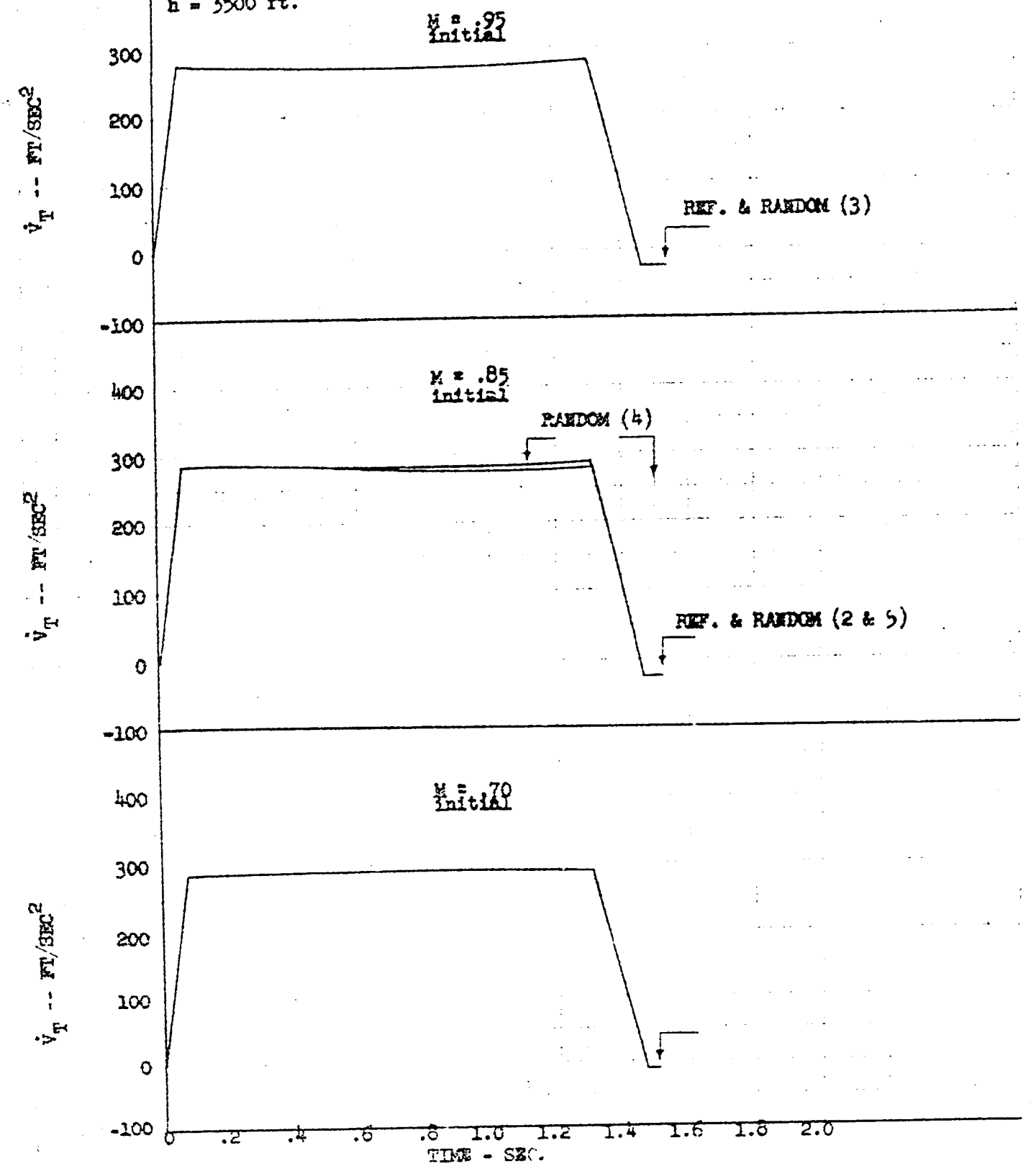

Figure 4.12

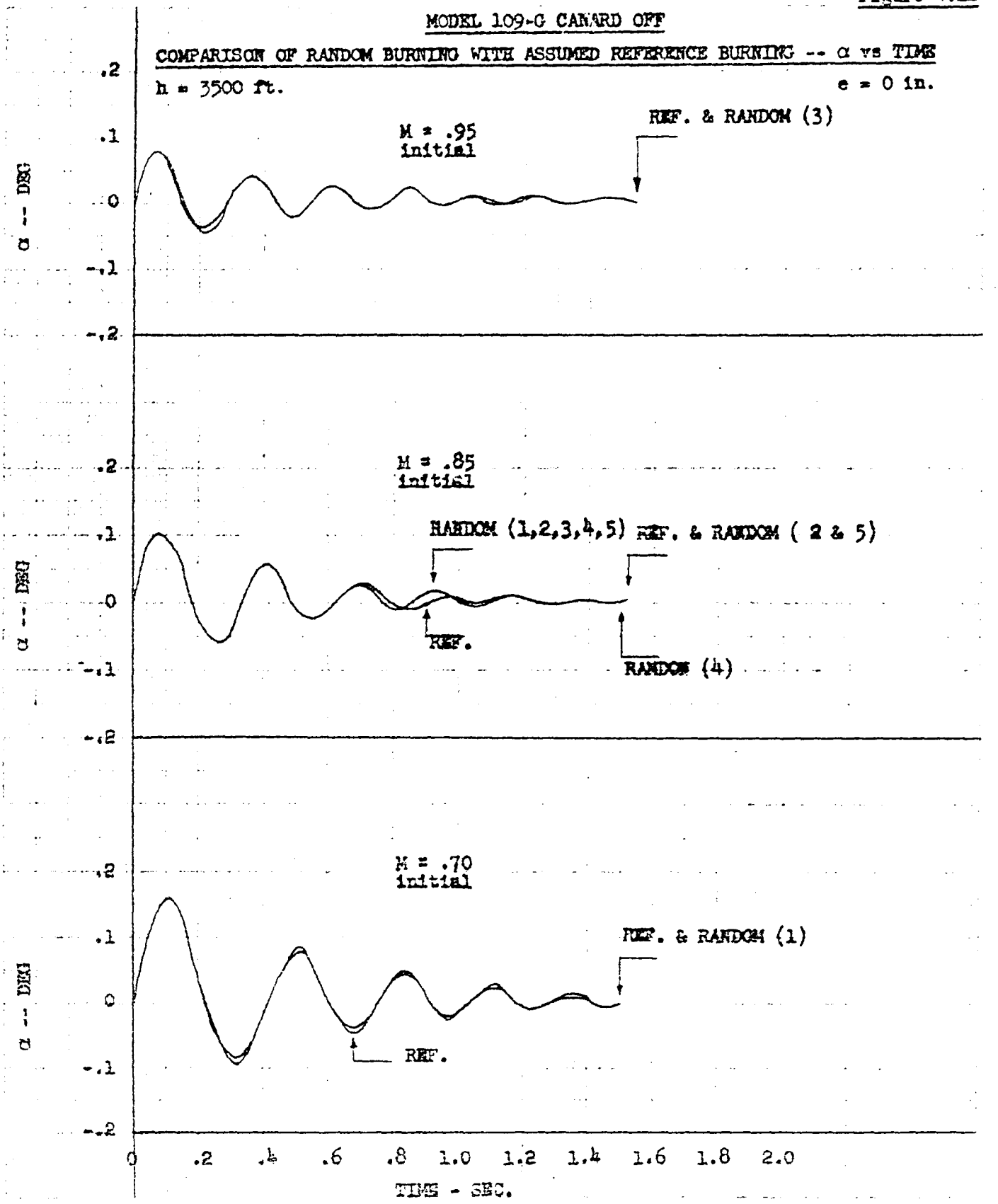
MODEL 109-G CANARD OFF
COMPARISON OF RANDOM BURNING WITH ASSUMED REFERENCE BURNING -- α vs TIME
h = 3500 ft.
e = 0 in.
M = .95
initial
REF. & RANDOM (3)
M = .85
initial
RANDOM (1,2,3,4,5)
REF. & RANDOM (2 & 5)
REF.
RANDOM (4)
M = .70
initial
REF. & RANDOM (1)
REF.
α -- DEG
.2
.1
0
-.1
-.2
0
.2
.4
.6
.8
1.0
1.2
1.4
1.6
1.8
2.0
TIME - SEC.

Figure 4.13

MODEL 109-G CANARD OFF

COMPARISON OF RANDOM BURNING WITH ASSUMED REFERENCE BURNING -- $\dot{\theta}$ vs TIME

h = 3500 ft. e = 0 in.

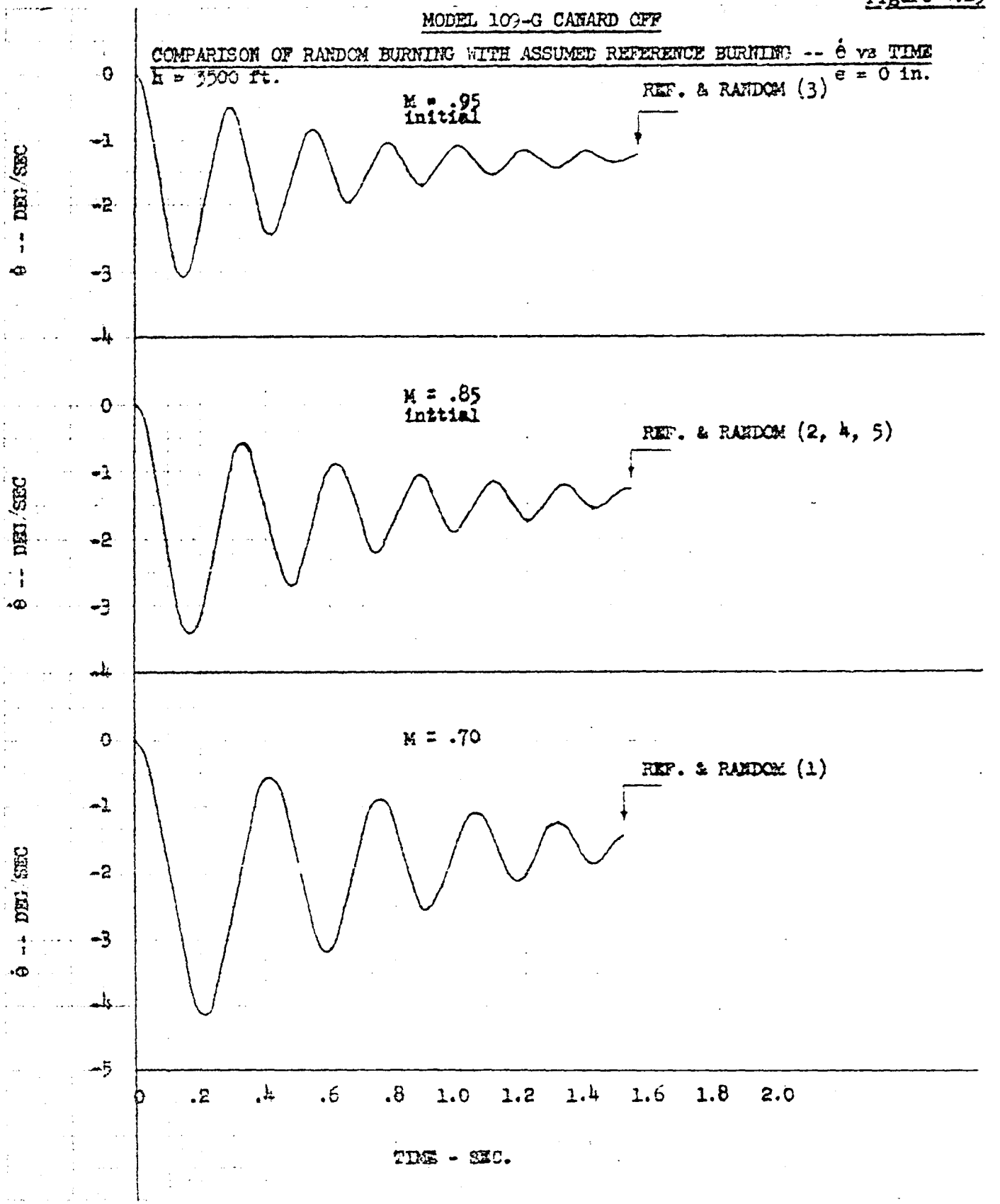

Figure 4.14

MODEL 109-G CANARD OFF

COMPARISON OF RANDOM BURNING WITH ASSUMED REFERENCE BURNING -- $\ddot{\theta}$ vs TIME

h = 5500 ft. e = 0 in.

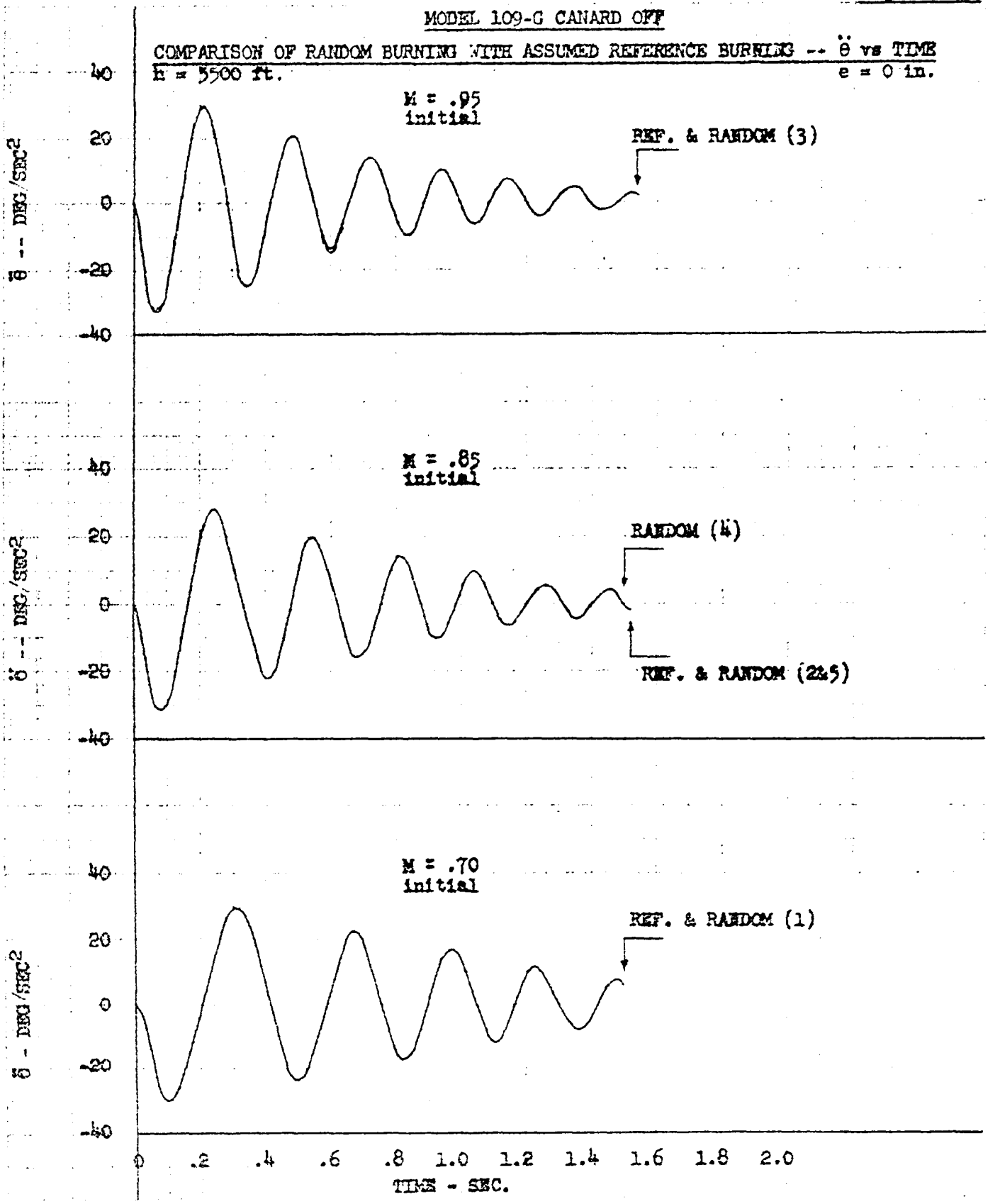

Figure 4.15

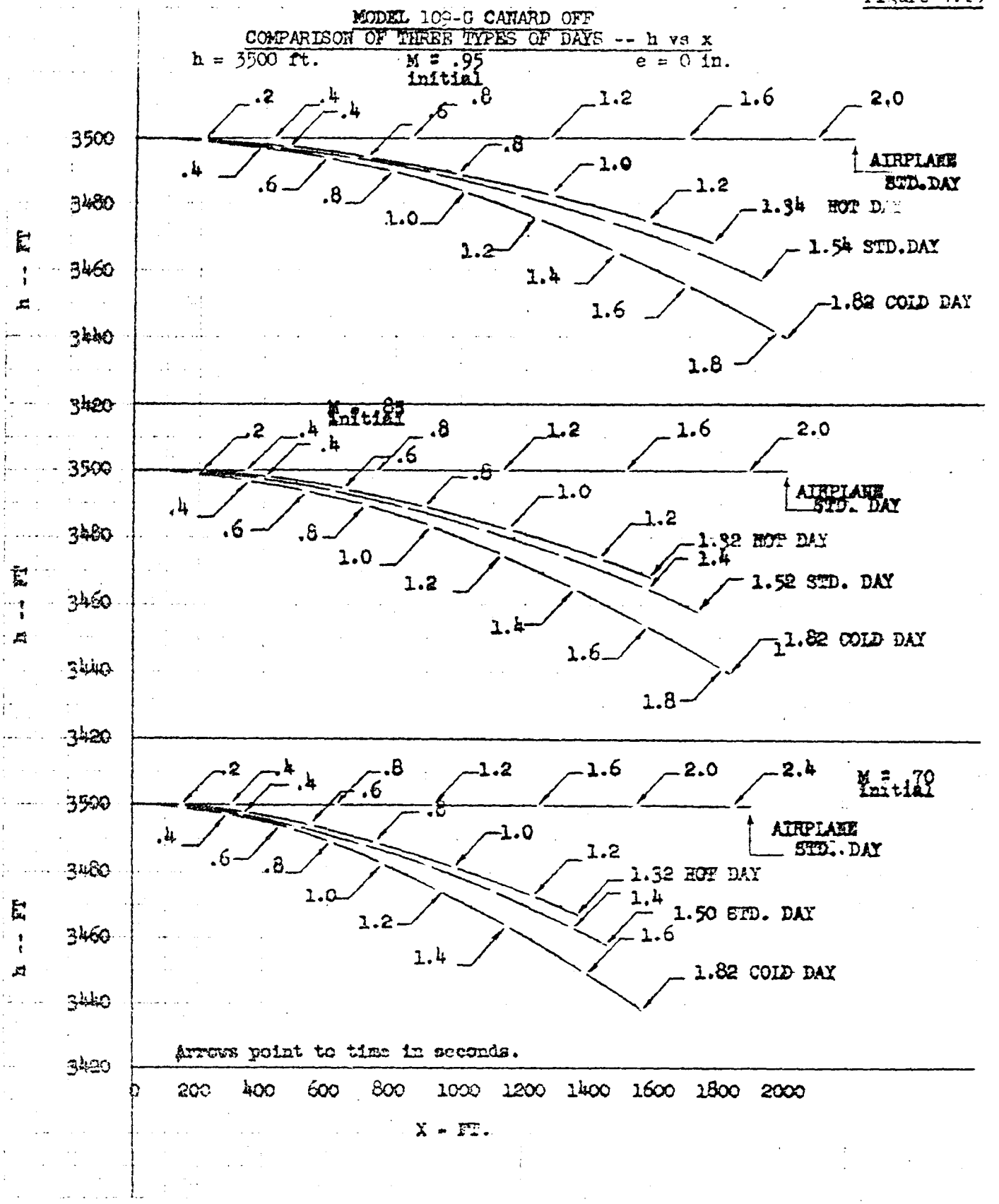
MODEL 109-G CANARD OFF
COMPARISON OF THREE TYPES OF DAYS -- h vs x
h = 3500 ft.
M = .95 initial
e = 0 in.
AIRPLANE STD.DAY
1.34 HOT DAY
1.54 STD.DAY
1.82 COLD DAY
M = .85 initial
AIRPLANE STD. DAY
1.32 HOT DAY
1.52 STD. DAY
1.82 COLD DAY
M = .70 initial
AIRPLANE STD. DAY
1.32 HOT DAY
1.50 STD. DAY
1.82 COLD DAY
Arrows point to time in seconds.
h - FT.
X - FT.

Figure 4.16

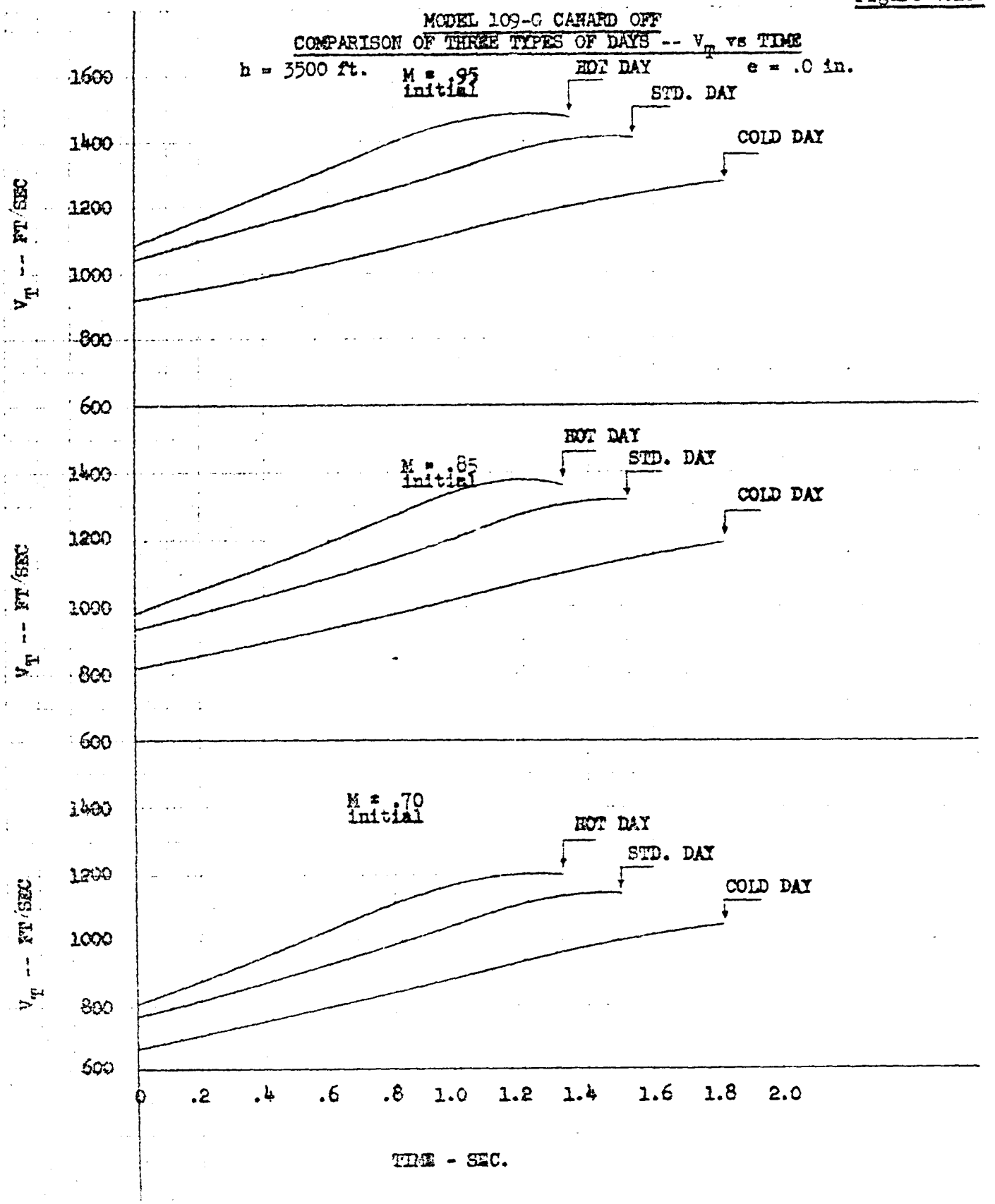
MODEL 109-G CANARD OFF
COMPARISON OF THREE TYPES OF DAYS -- V_T vs TIME
h = 3500 ft.
e = .0 in.
M = .95 initial
HOT DAY
STD. DAY
COLD DAY
M = .85 initial
HOT DAY
STD. DAY
COLD DAY
M = .70 initial
HOT DAY
STD. DAY
COLD DAY
V_T -- FT/SEC
1600
1400
1200
1000
800
600
0
.2
.4
.6
.8
1.0
1.2
1.4
1.6
1.8
2.0
TIME - SEC.

Figure 4.17

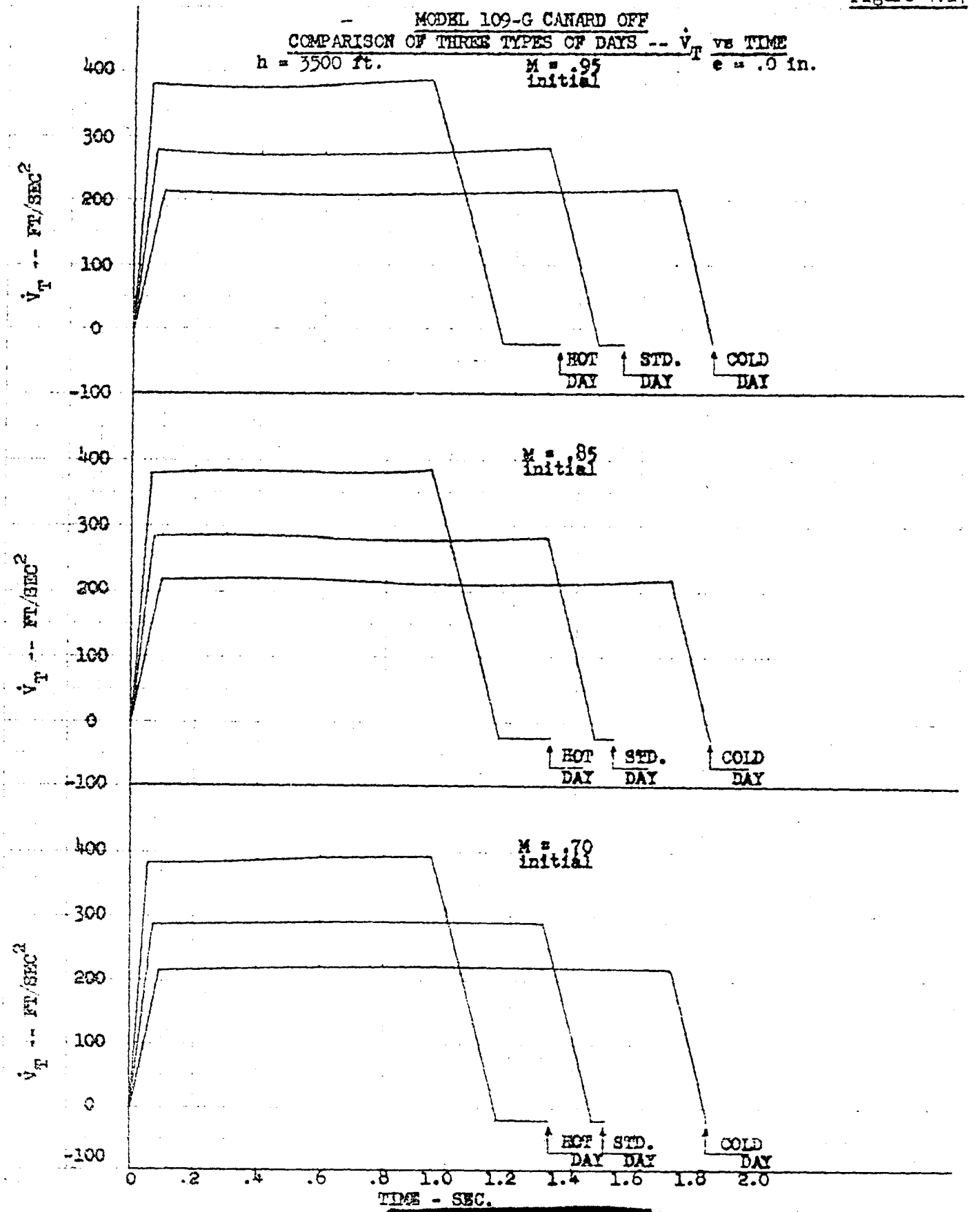
MODEL 109-G CANARD OFF
COMPARISON OF THREE TYPES OF DAYS -- $\dot{V}_T$ vs TIME
h = 3500 ft.
M = .95 initial
e = .0 in.
M = .85 initial
M = .70 initial
HOT DAY
STD. DAY
COLD DAY
$\dot{V}_T$ -- FT/SEC^2
400
300
200
100
0
-100
0
.2
.4
.6
.8
1.0
1.2
1.4
1.6
1.8
2.0
TIME - SEC.

Figure 4.18

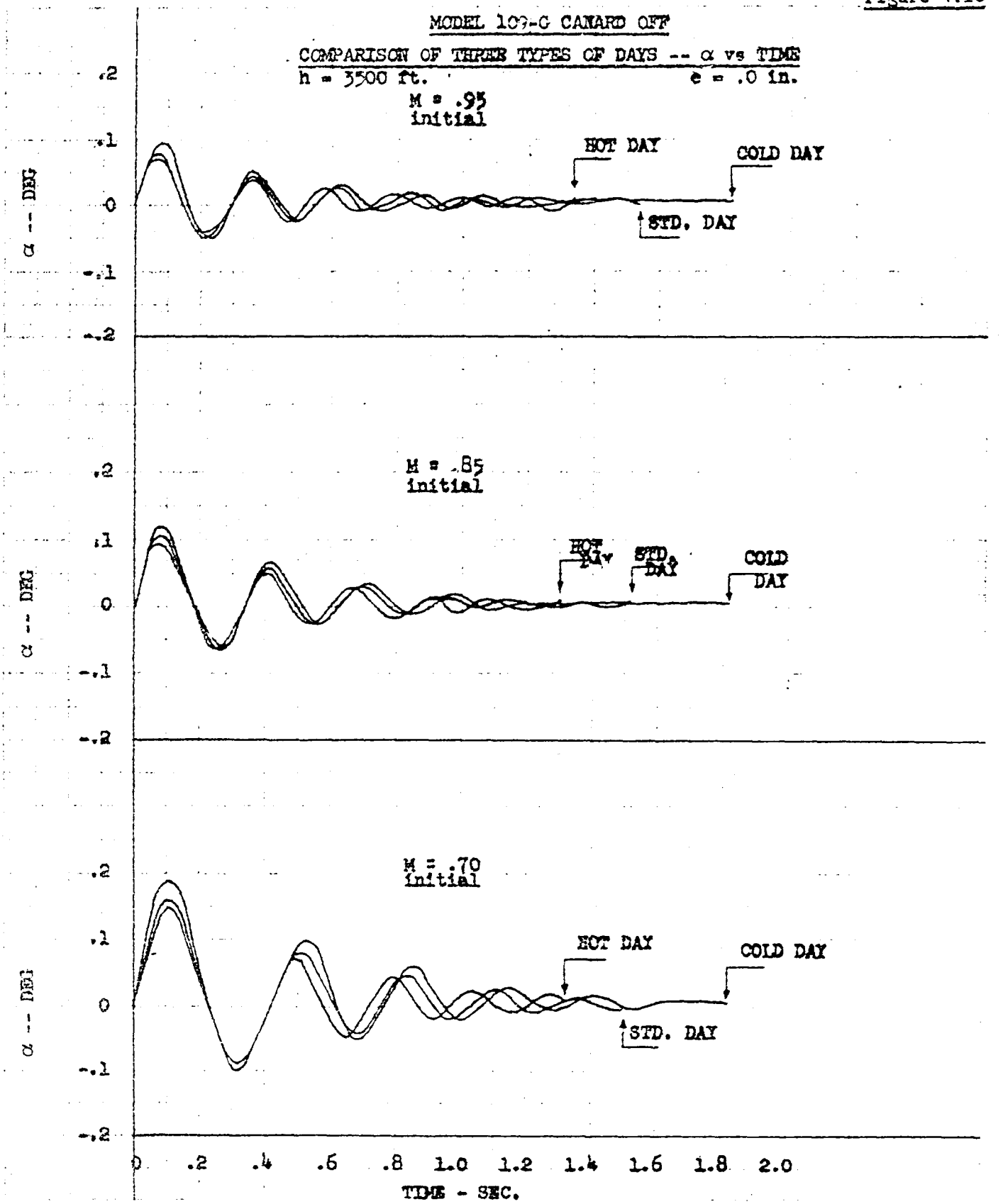
MODEL 109-C CANARD OFF
COMPARISON OF THREE TYPES OF DAYS -- α vs TIME
h = 3500 ft.
e = .0 in.
M = .95
initial
HOT DAY
COLD DAY
STD. DAY
M = .85
initial
HOT DAY
STD. DAY
COLD DAY
M = .70
initial
HOT DAY
COLD DAY
STD. DAY
α -- DEG
.2
.1
0
-.1
-.2
0
.2
.4
.6
.8
1.0
1.2
1.4
1.6
1.8
2.0
TIME - SEC.

Figure 4.19

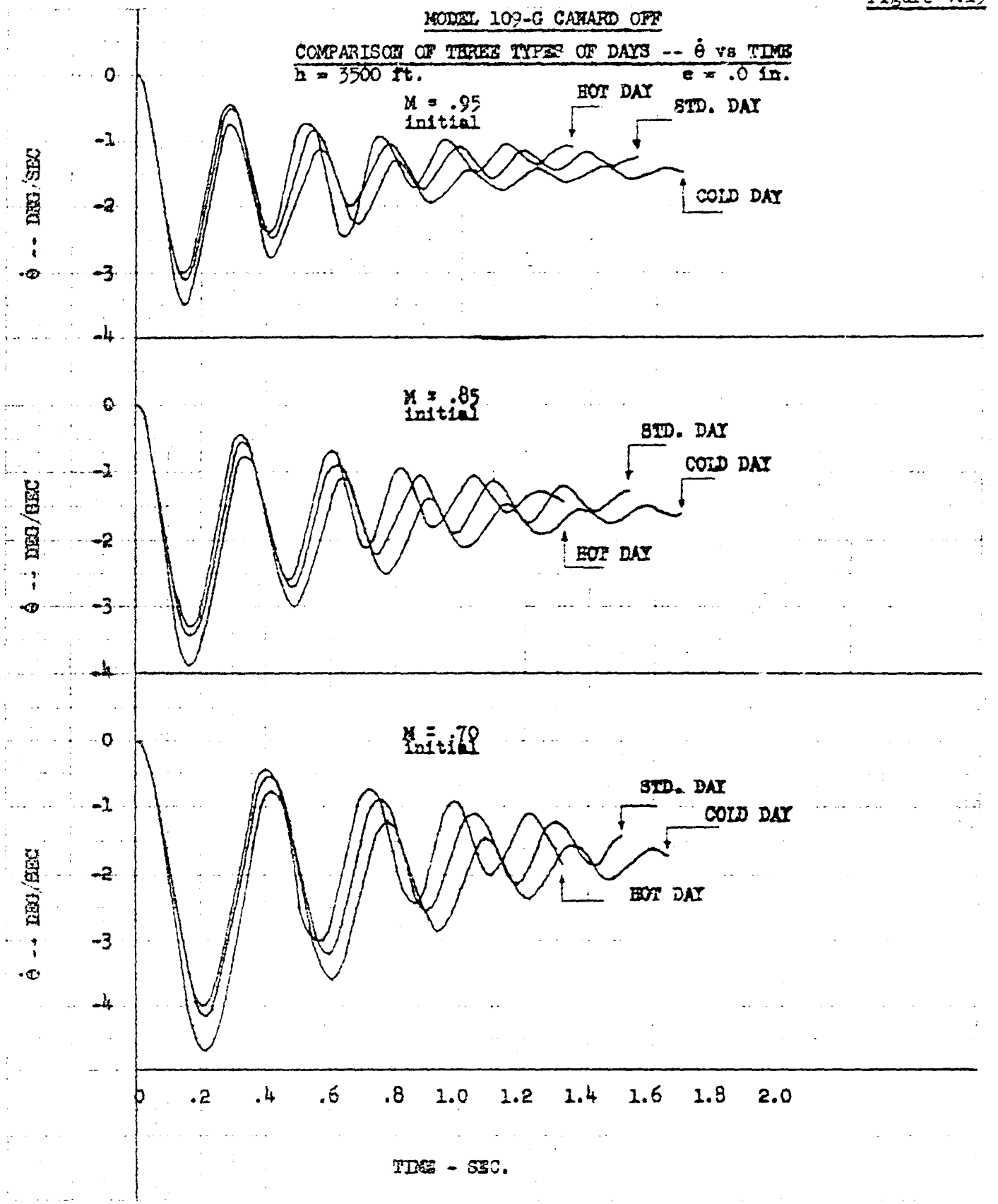
MODEL 109-G CANARD OFF
COMPARISON OF THREE TYPES OF DAYS -- θ̇ vs TIME
h = 3500 ft.
e = .0 in.
M = .95
initial
HOT DAY
STD. DAY
COLD DAY
M = .85
initial
STD. DAY
COLD DAY
HOT DAY
M = .70
initial
STD. DAY
COLD DAY
HOT DAY
θ̇ - DEG/SEC
0
-1
-2
-3
-4
0
.2
.4
.6
.8
1.0
1.2
1.4
1.6
1.8
2.0
TIME - SEC.

Figure 4.20

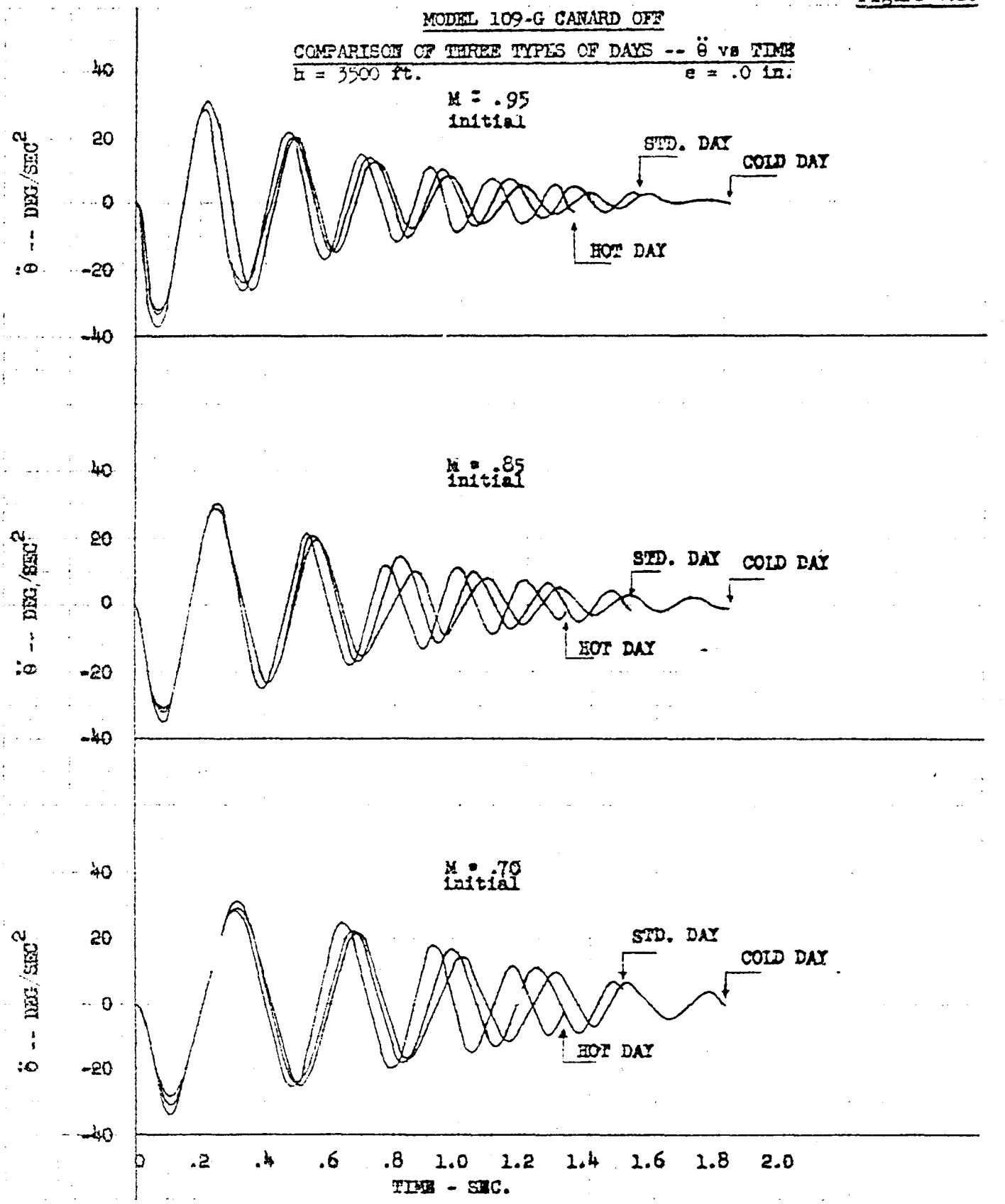
MODEL 109-G CANARD OFF
COMPARISON OF THREE TYPES OF DAYS -- θ̈ vs TIME
h = 3500 ft.
e = .0 in.
M = .95
initial
STD. DAY
COLD DAY
HOT DAY
M = .85
initial
STD. DAY
COLD DAY
HOT DAY
M = .70
initial
STD. DAY
COLD DAY
HOT DAY
θ̈ -- DEG/SEC²
40
20
0
-20
-40
0
.2
.4
.6
.8
1.0
1.2
1.4
1.6
1.8
2.0
TIME - SEC.

Figure 4.21

MODEL 109-G CANARD OFF

COMPARISON OF THREE VERTICAL THRUST LINE LOCATIONS -- h vs x

h = 3500 ft. Std. Day

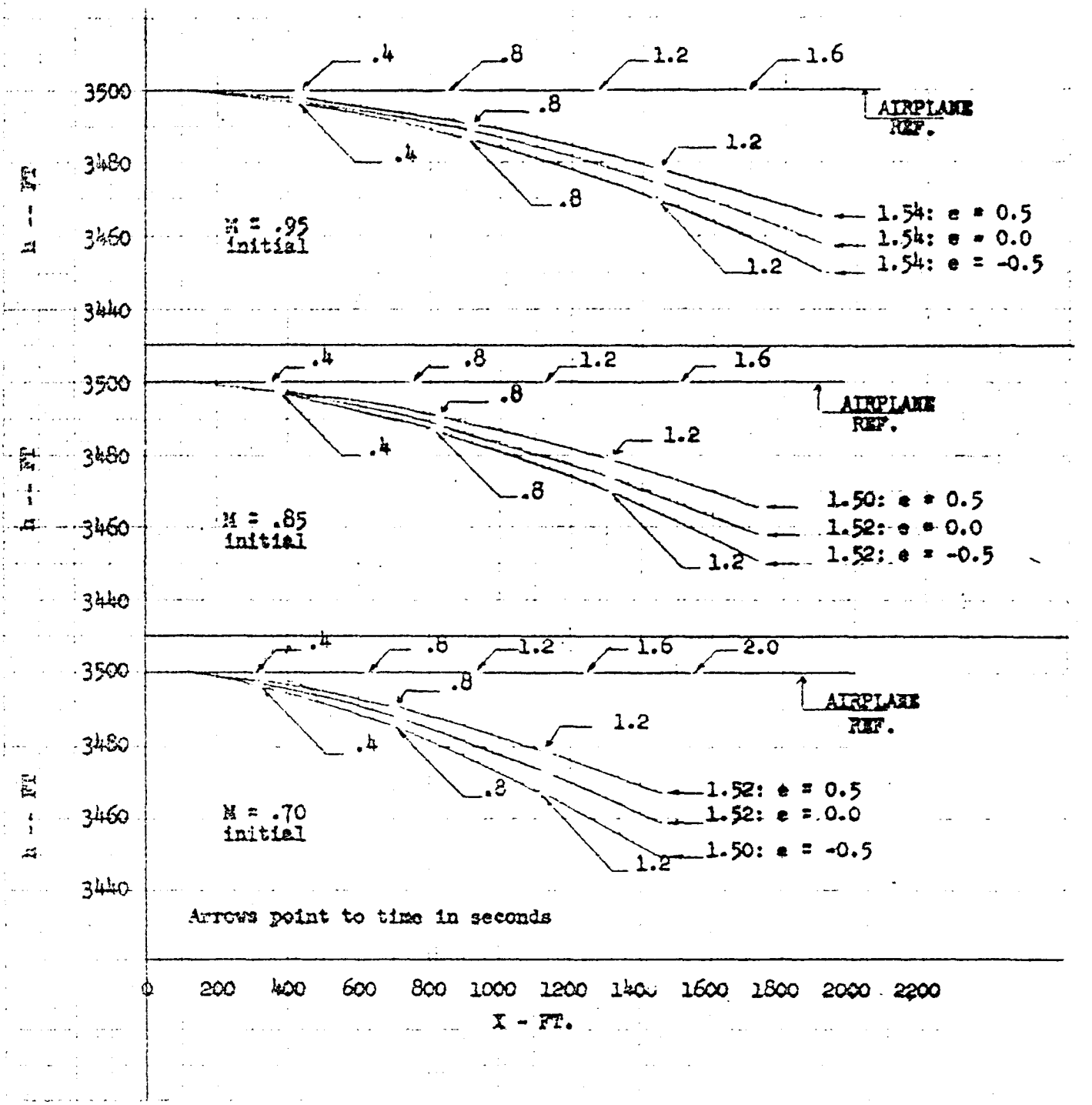

Figure 4.22

MODEL 109-G CANARD OFF

COMPARISON OF THREE VERTICAL THRUST LINE LOCATIONS -- V_T vs TIME

M = 3500 ft. Std. Day

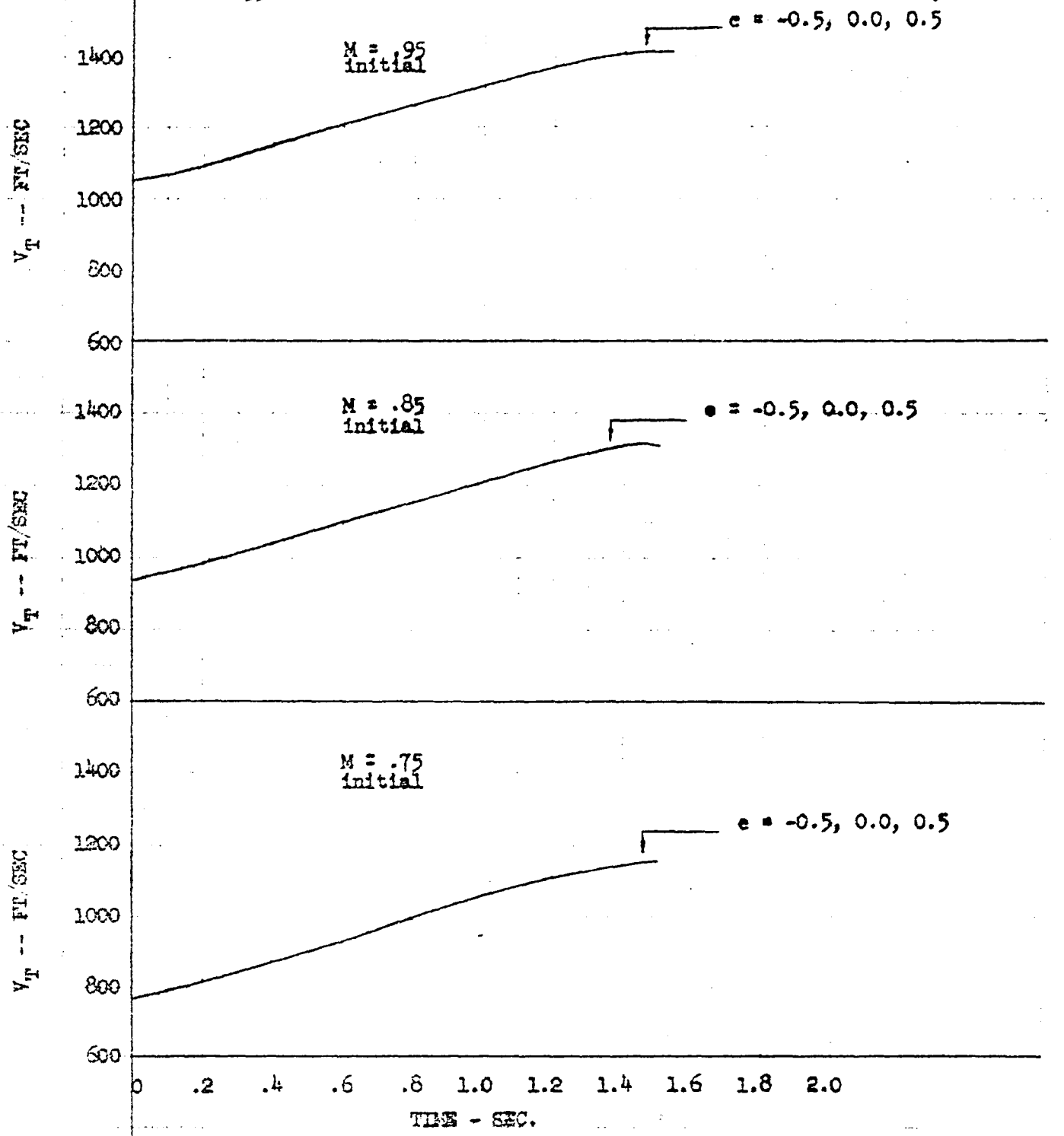

Figure 4.23

MODEL 109-G CANARD OFF

COMPARISON OF THREE VERTICAL THRUST LINE LOCATIONS -- $\dot{V}_T$ vs TIME

h = 3500 ft. Std. Day

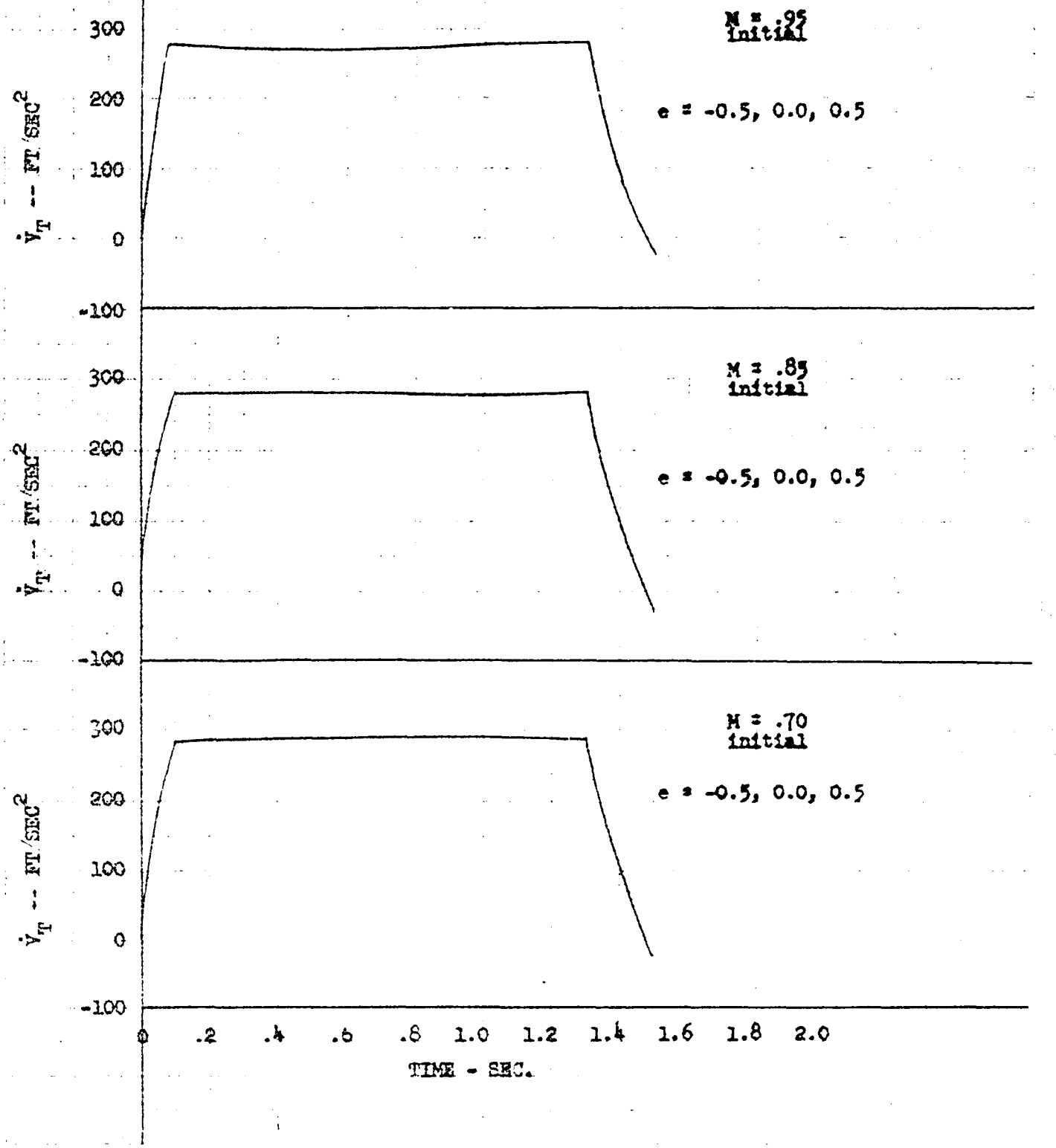

Figure 4.24

MODEL 109-G CANARD OFF

COMPARISON OF THREE VERTICAL THRUST LINE LOCATIONS -- α vs TIME

h = 3500 ft. Std. Day

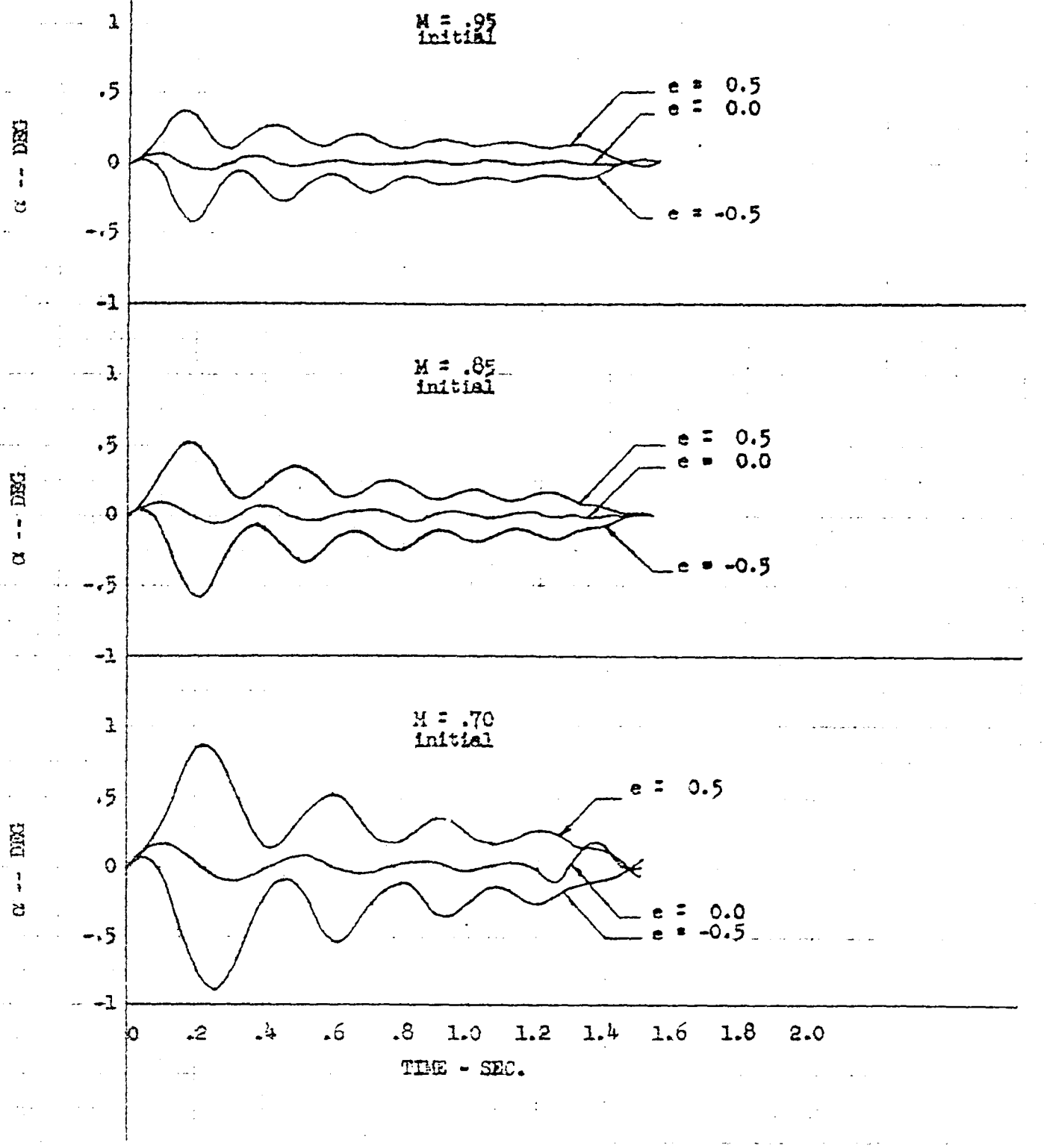

Figure 4.25

MODEL 100-G CANARD OFF

COMPARISON OF THREE VERTICAL THRUST LINE LOCATIONS -- $\dot{\theta}$ vs TIME

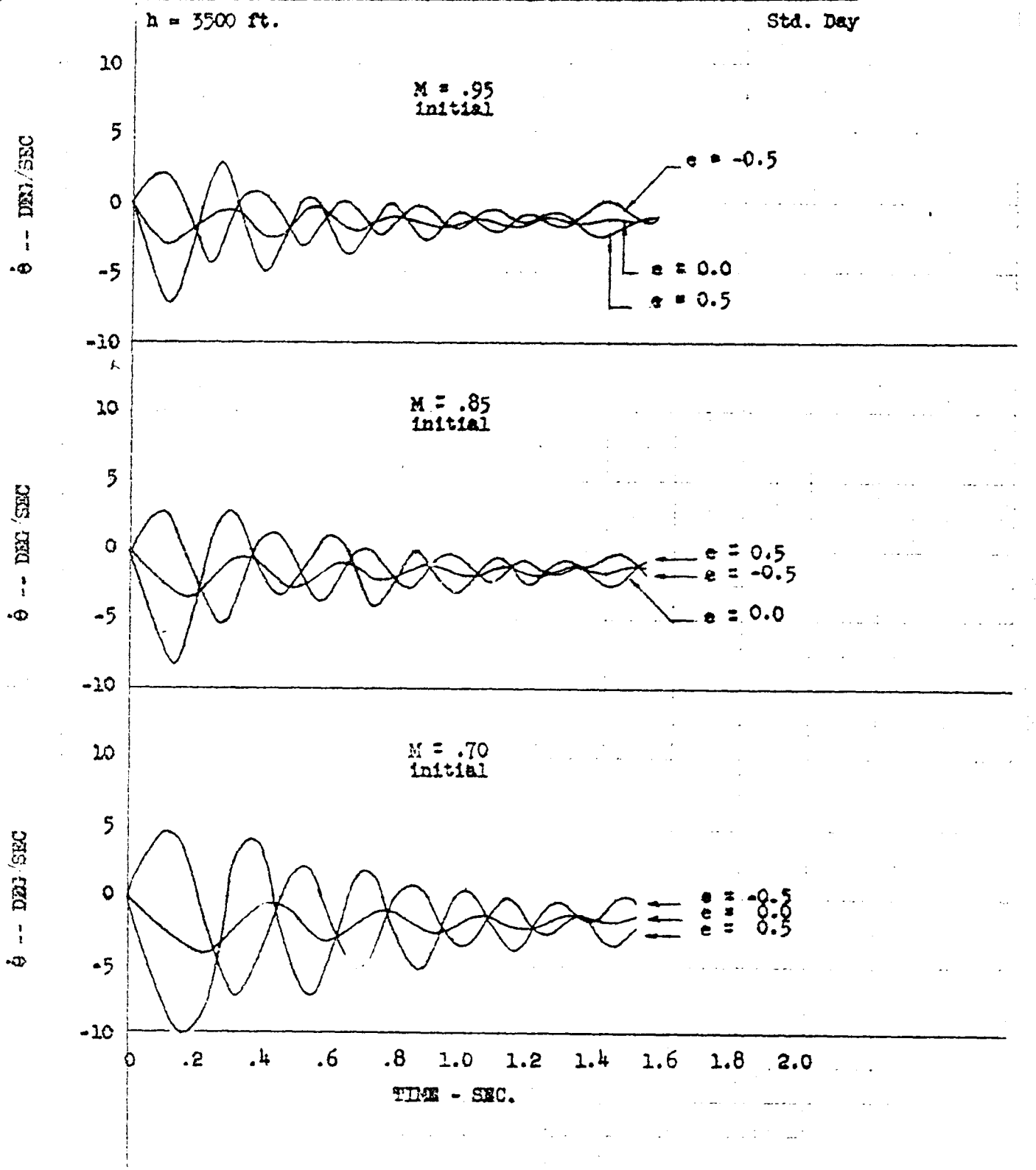

Figure 4.26

MODEL 109-G CANARD OFF

COMPARISON OF THREE VERTICAL THRUST LINE LOCATIONS -- $\ddot{\theta}$ vs TIME

h = 3500 ft. Std. Day

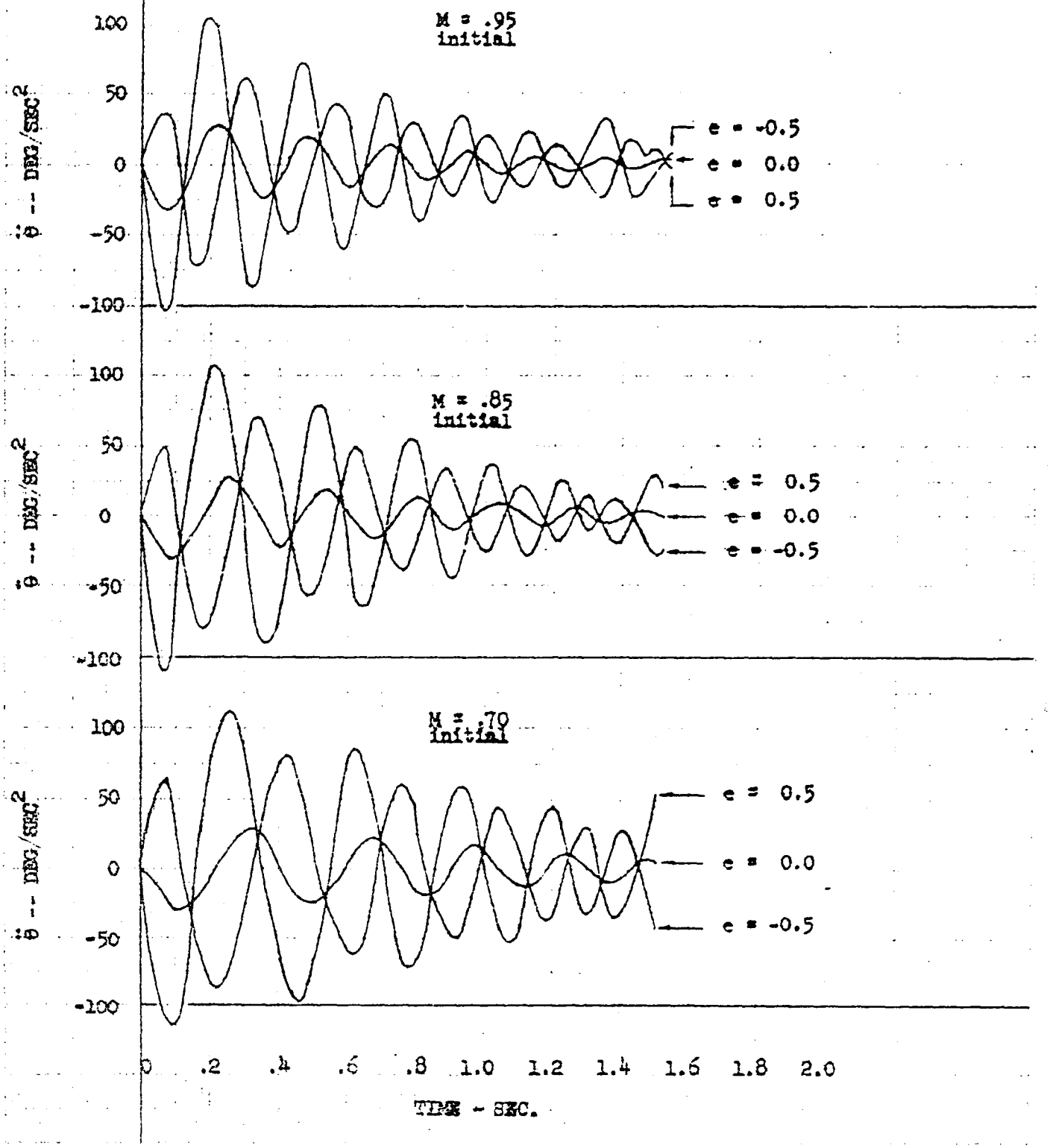

Figure 4.27

MODEL 109-G CANARD OFF

COMPARISON OF THREE LATERAL THRUST LINE LOCATIONS -- y vs x

h = 3500 ft. $\bar{e}$ = 0.5 in.

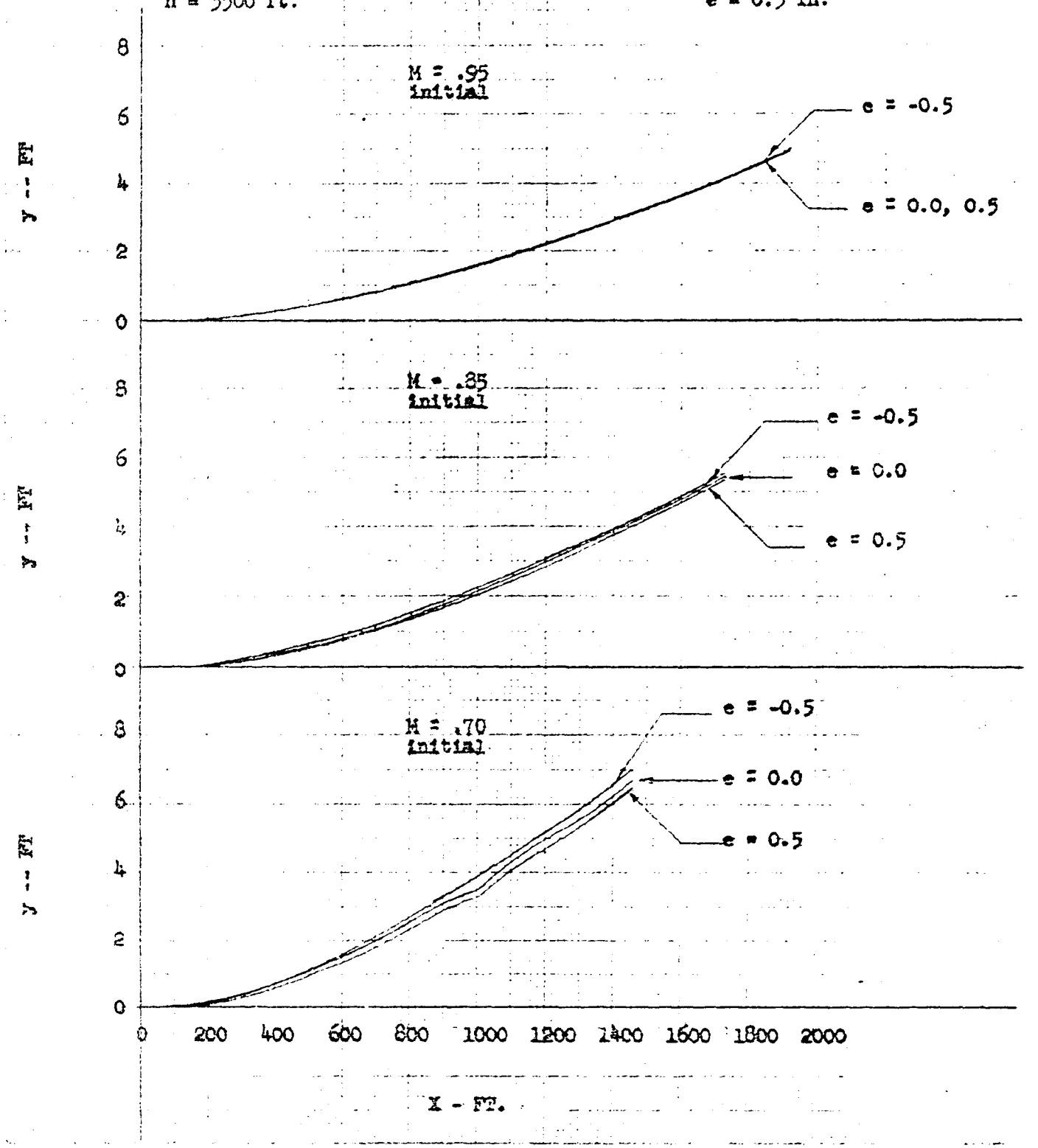

Figure 4.28

MODEL 109-G CANARD OFF

COMPARISON OF THREE LATERAL THRUST LINE LOCATIONS -- $\dot{V}$ vs TIME

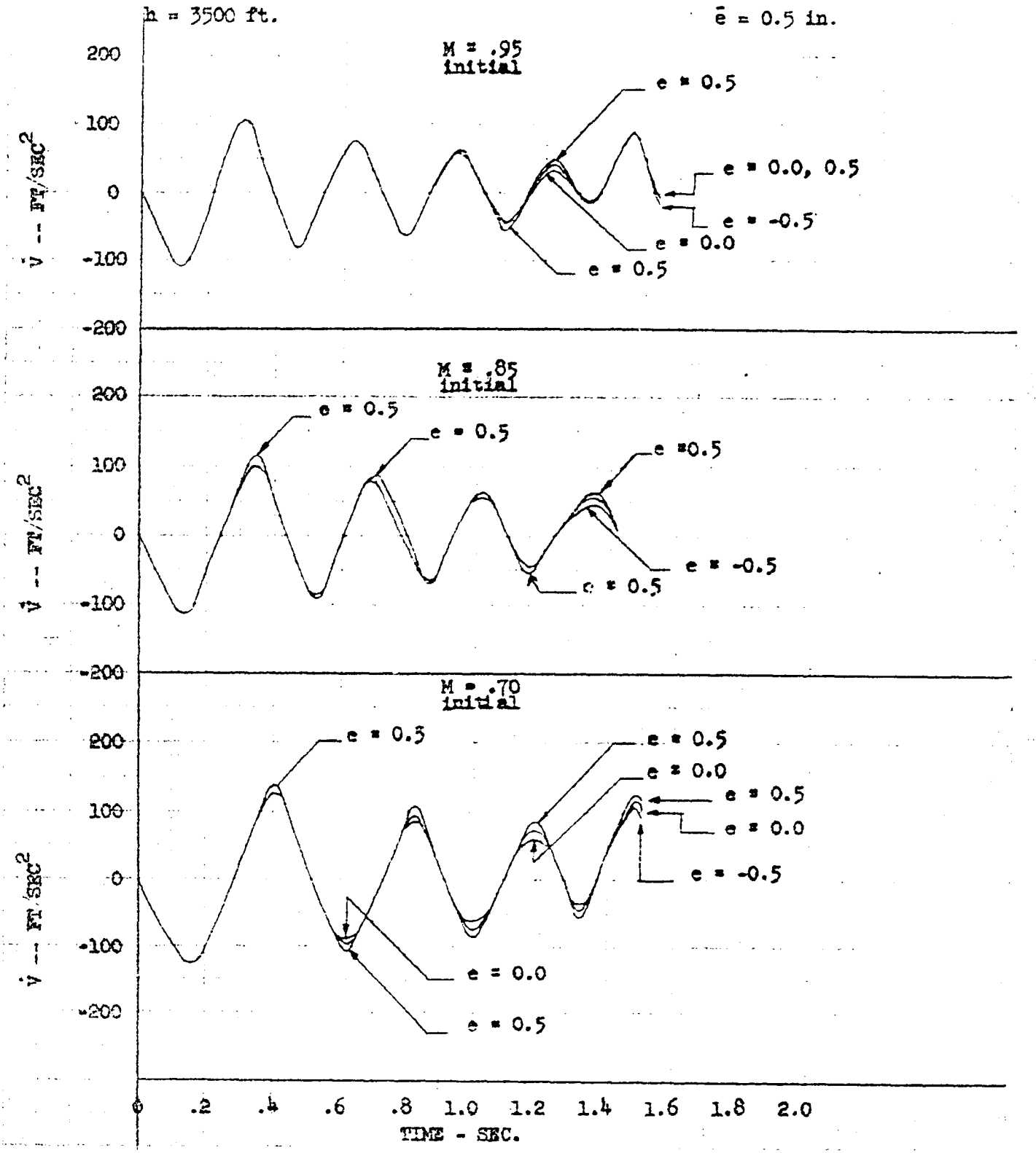

Figure 4.29

MODEL 109-G CANARD OFF

COMPARISON OF THREE LATERAL THRUST LINE LOCATIONS -- ϕ vs TIME

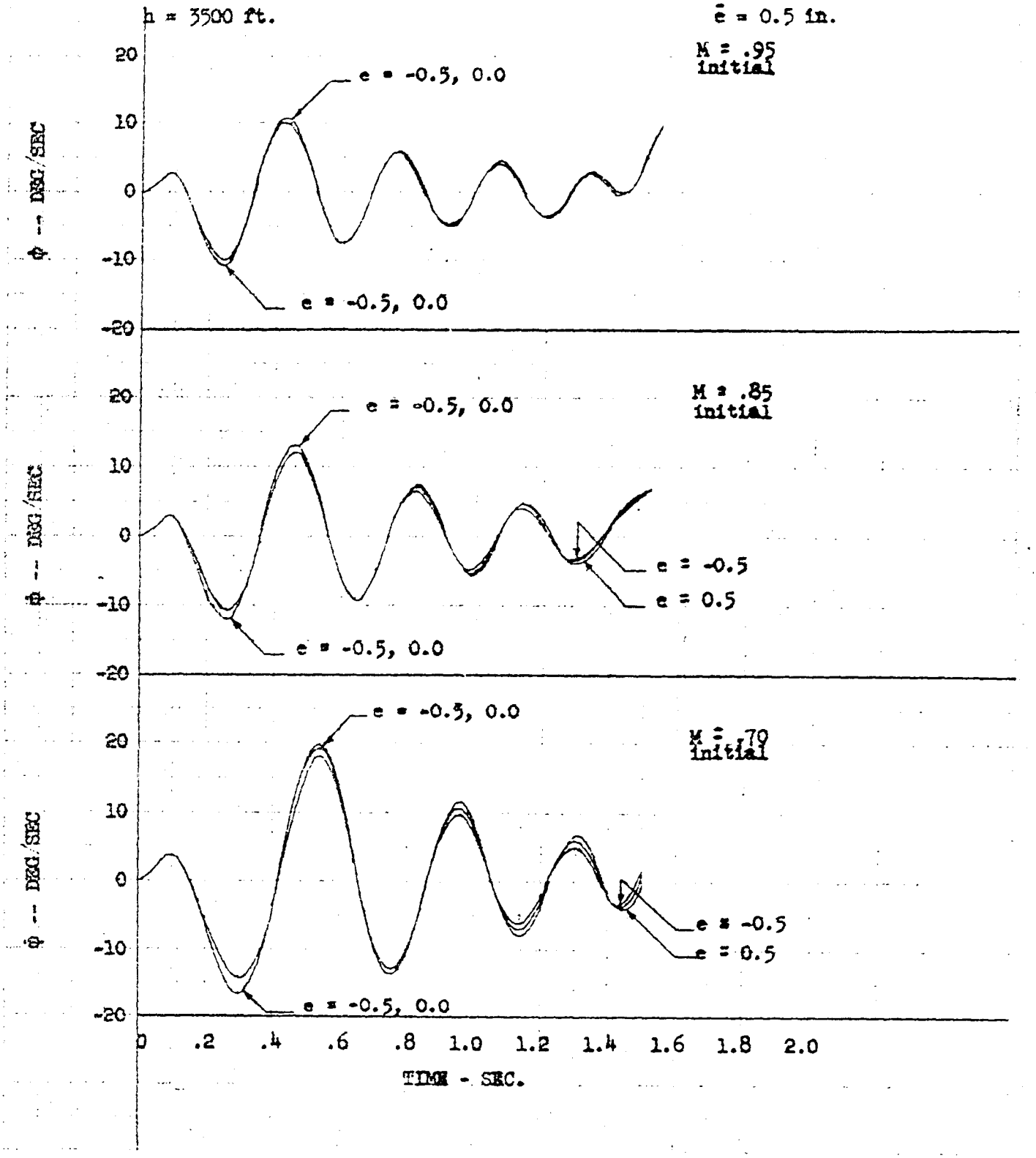

Figure 4.30

MODEL 109-G CANARD OFF

COMPARISON OF THREE LATERAL THRUST LINE LOCATIONS -- $\ddot{\Phi}$ vs TIME

h = 3500 ft. Φ = 0.5 in.

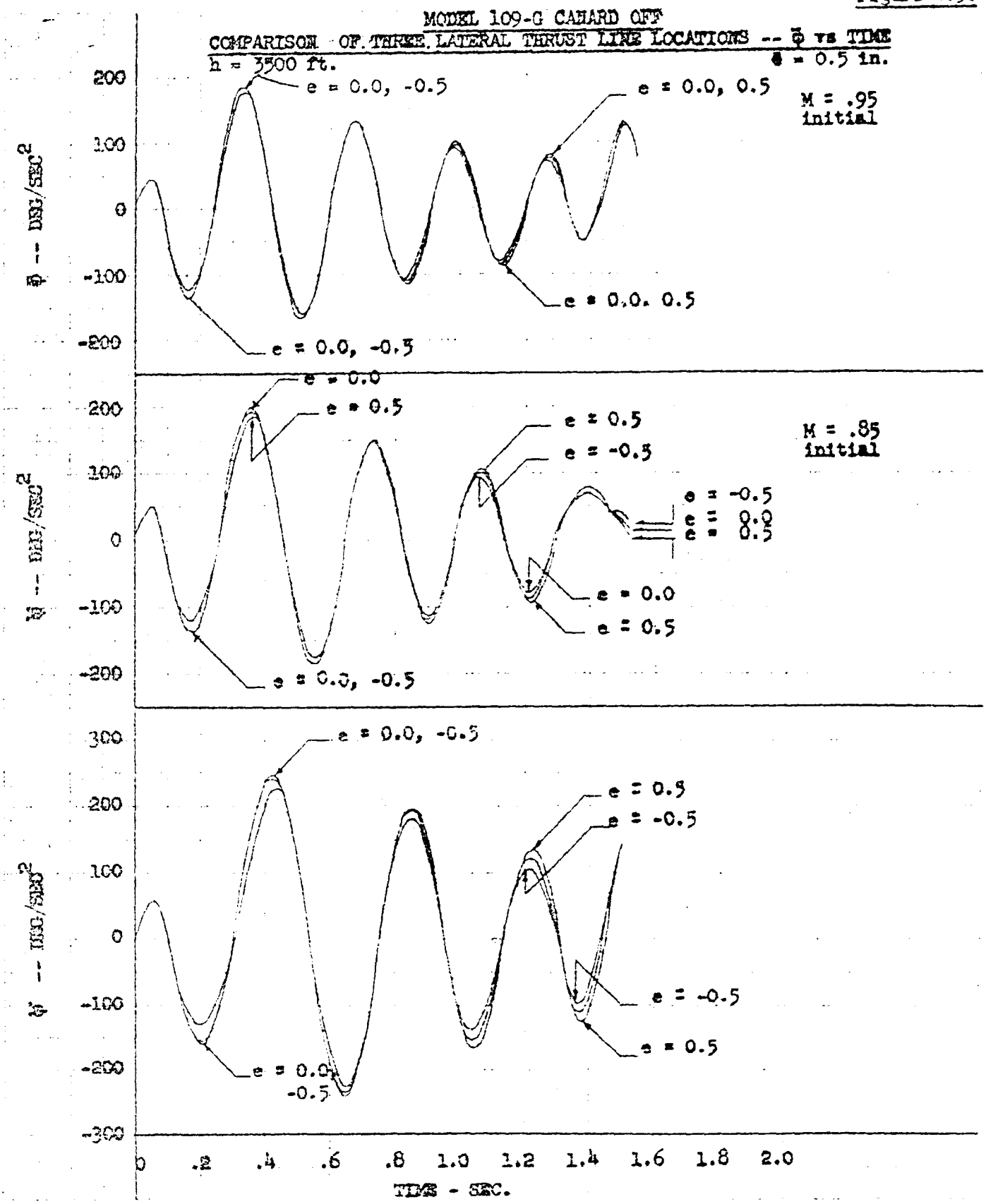

Figure 4.31

MODEL 109-G CANARD OFF

COMPARISON OF THREE LATERAL THRUST LINE LOCATIONS -- $\dot{\psi}$ vs TIME

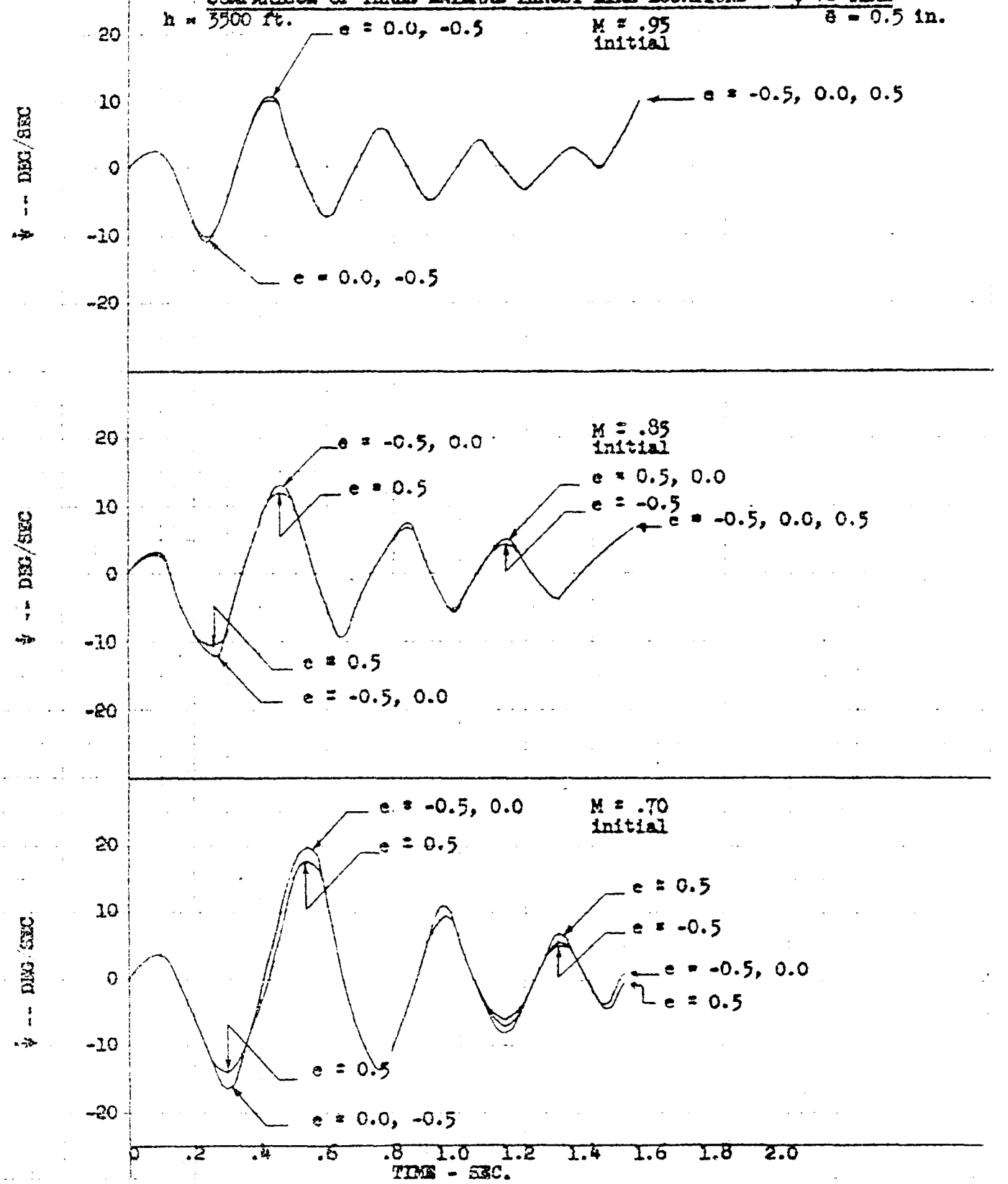

Figure 4.32

MODEL 109-G CANARD OFF

COMPARISON OF THREE LATERAL THRUST LINE LOCATIONS -- $\ddot{\psi}$ vs TIME

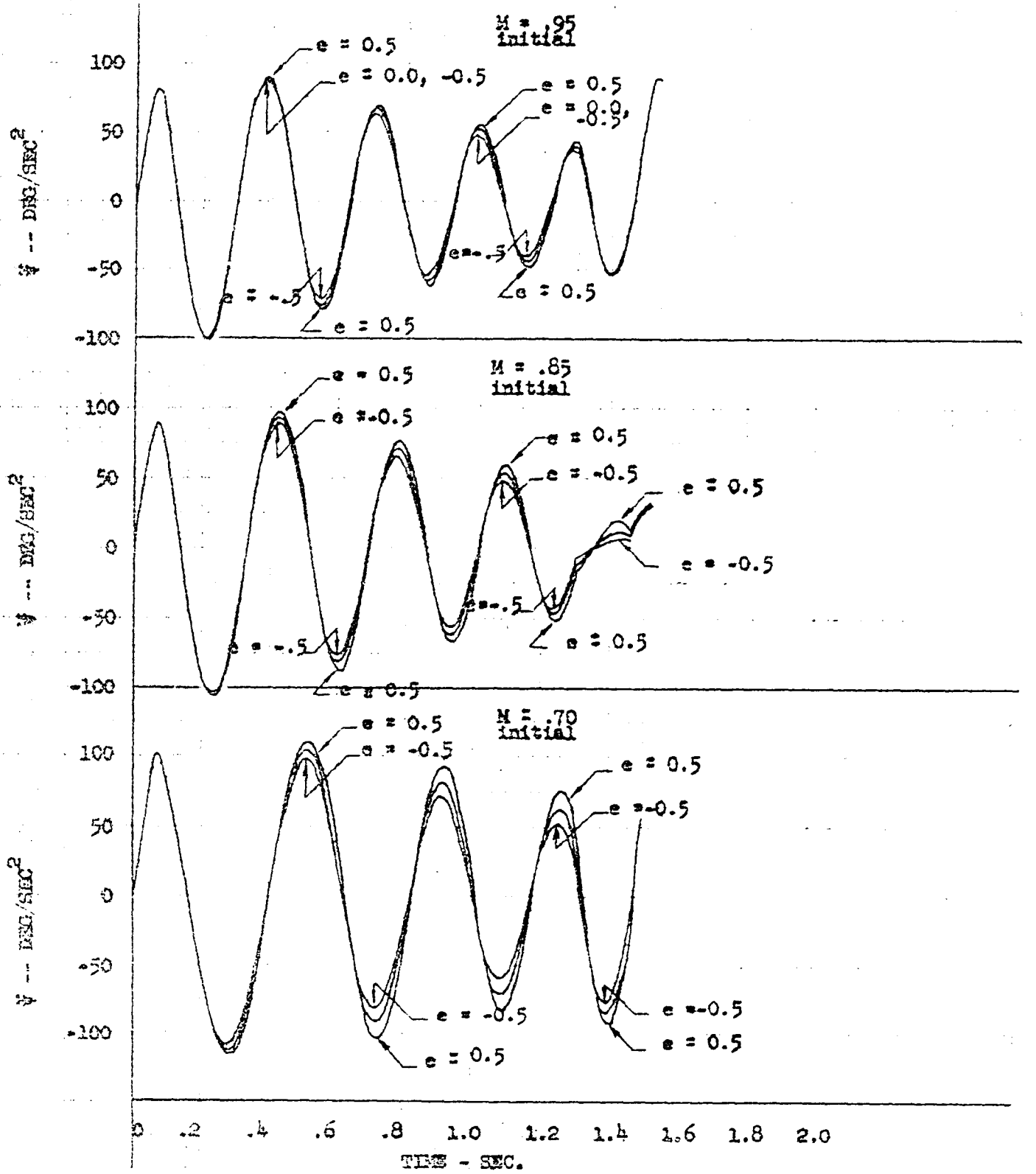

5.0 CONCLUSIONS

Even the most unfavorable assumptions of faulty rocket performance or structural imperfections failed to yield radial displacements approaching the magnitude allowed. It may be concluded that the Model 109-G is capable of producing repeatable trajectories with the accuracy demanded by the Phase I ballistic CEP requirements.

6.0 APPENDIX

Presented in the Appendix are the following sections:

6.1 List of References

6.2 List of Symbols

6.3 Equations

6.1 List of References

1. Sandia Corporation: Purchase Order to Ryan Aeronautical Company, Number 51-2116, 25 May 1956, Unclassified.

2. Craig, D. R.: Proposal for the Extension of the Phase I CEP Studies for LOTOP Project (Ryan Model 109), Ryan Report 10918-4, 11 December 1956, Confidential.

3. McGovern, J. E.: Change in Emphasis in LOTOP Project, Sandia Corporation letter, 2 November 1956, Confidential.

4. Richert, J. J.: Change in Emphasis on LOTOP Project, Ryan letter, 23 November 1956, Confidential.

5. Hughes, J. W.: Change in Emphasis on LOTOP Project, Sandia Corporation letter, 5 December 1956, Unclassified.

6. Solid Propellant Information Agency: JATO Manual SPIA/M1, Applied Physics Laboratory, The Johns Hopkins University, Maryland, 1956, Confidential.

7. Hansen, H. J., Inman, D. C., and Britt, D. L.: Preliminary System Analysis, Phase I, LOTOP Project, Ryan Report 10955-1, 11 January 1957, Confidential.

6.2 List of Symbols

D	Drag, lbs.
F_n	Net thrust, lbs.
L	Lift, lbs.
M_{Aero}	Aerodynamic pitching moment, ft. lbs.
W	Weight, lbs.
g	Gravitational acceleration, 32.17405 ft/sec^2
n	Load factor, $\frac{\text{Sum of all forces normal to flt. path exclusive of } W \cos \gamma}{W}$
I_{x_b}	Moment of inertia about longitudinal body axis, slug ft.^{2}
I_{y_b}	Moment of inertia about spanwise body axis, slug ft.^{2}
I_{xz_b}	Product of inertia, slug ft.^{2}
b	Wing span, ft.
θ	Pitch angle referenced to horizontal plane, radians
$\dot{\theta}$	$d\theta/dt$, rad./sec.
$\ddot{\theta}$	$d\dot{\theta}/dt$, rad. sec.^{2}
γ	Flight path angle referenced to horizontal plane, radians
$\dot{\gamma}$	$d\gamma/dt$, rad./sec.
α	Angle of attack, i.e. angle between wing chord plane and flight path, rad.
α_{OL}	α for zero lift, radians
$\dot{\alpha}$	$d\alpha/dt$, rad./sec.
β	Side-slip angle, i.e., angle between longitudinal body axis and relative wind, radians
φ	Roll angle referenced to horizontal plane, radians
$\dot{\varphi}$	$d\varphi/dt$, rad./sec.
$\ddot{\varphi}$	$d\dot{\varphi}/dt$, rad./sec.^{2}

ψ	Yaw angle referenced to fixed vertical plane, radians
$\dot{\psi}$	$d\psi/dt$, rad./sec.
$\ddot{\psi}$	$d\dot{\psi}/dt$, rad./sec.^{2}
v	Velocity along Y_b axis, ft./sec.
$\dot{v}$	dv/dt, ft./sec.^{2}
δ_a	Aileron deflection, radians
δ_r	Deflection of vertical canard surface, radians
δ_e	Deflection of horizontal canard surface, degrees
e	Vertical thrust moment arm about c.g., ft.
$\bar{e}$	Lateral thrust moment arm about c.g., ft.
$K_{\phi\delta_a}$	Aileron to roll gain
$K_{\dot{\phi}\delta_a}$	Aileron to roll rate gain
$K_{\psi\delta_r}$	Vertical canard surface deflection to yaw gain
u	Velocity along X_b axis, ft./sec.
w	Velocity along Z_b axis, ft./sec.
x, y, h	Cartesian coordinates with respect to ground, ft.
$\dot{x}, \dot{y}, \dot{h}$	dx/dt, dy/dt, dh/dt, ft./sec.
X_b, Y_b, Z_b	Body axes
c.g.	Stationwise location of center of gravity, inches
S	Wing planform area, ft.^{2}
q	Dynamic pressure, $\rho V_T^2/2$, lbs./ft.^{2}
q_c	Impact pressure $q(1 + \frac{M^2}{4} + \frac{M^4}{40} + \frac{M^6}{1600}$ etc.), lbs./ft.^{2}
V_T	Freestream velocity, ft./sec.
$\dot{V}_T$	dV_T/dt, ft./sec.^{2}
ρ	Ambient density, slugs/ft.^{3}

$\bar{c}$	Mean aerodynamic chord, ft.
d_c	Clearance distance from missile c.g. to launch point on launch aircraft, ft.
D_c	Arbitrarily chosen clearance distance at which maneuver may be commenced, ft.
M	Mach number
t	Time, seconds
C_L	Lift coefficient, L/qs
C_D	Total drag coefficient, D/qS
$C_{D_{\delta_e = 0}}$	C_D at $\delta_e = 0$
C_m	Pitching moment coefficient, Pitching moment $/qS\bar{c}$
C_{m_o}	Pitching moment coefficient at $\alpha = 0$
$C_{L\alpha}$	$\partial C_L/\partial\alpha$
$C_{L_{\delta_e = 0}}$	C_L at $\delta_e = 0$
C_{m_α}	$\partial C_m/\partial\alpha$
C_{m_q}	$\partial C_m/\partial\dot{\theta}$
$C_{m_{\dot{\alpha}}}$	$\partial C_m/\partial\dot{\alpha}$
C_y	Side force coefficient, $\frac{\text{side force}}{qS}$
C_{y_o}	Side force coefficient due to structural asymmetry
C_{y_β}	$\partial C_y/\partial\beta$
C_ℓ	Rolling moment coefficient, $\frac{\text{rolling moment}}{qSb}$
C_{ℓ_o}	Rolling moment coefficient due to structural asymmetry
C_{ℓ_β}	$\partial C_\ell/\partial\beta$
C_{ℓ_p}	$\partial C_\ell/\partial p$
C_{ℓ_r}	$\partial C_\ell/\partial r$
$C_{\ell_{\delta_a}}$	$\partial C_\ell/\partial\delta_a$

C_n	Yawing moment coefficient, $\frac{\text{yawing moment}}{qSb}$
C_{n_o}	Yawing moment coefficient due to structural asymmetry
C_{n_β}	$\partial C_n/\partial\beta$
C_{n_p}	$\partial C_n/\partial p$
C_{n_r}	$\partial C_n/\partial r$
C_{n}	$\partial C_n/\partial\delta_r$

6.3 Equations

6.3.1 Equations Used for Longitudinal Launch Studies - Canard Off

Summation of forces along the flight path:

$$\frac{W}{g}\dot{V}_T = F_n \cos(\alpha + i_{F_n}) - C_{D_{\delta_{e=0}}} qS - W \sin\gamma$$

Summation of forces normal to the flight path:

$$\frac{W}{g} V_T \dot{\gamma} = F_n \sin(\alpha + i_{F_n}) + C_{L_{\delta_{e=0}}} qS - W \cos\gamma$$

Summation of moments about the Y_b axis:

$$I_{y_b}\ddot{\theta} = eF_n + qS\bar{c}\left[C_{m_o} + C_{m_\alpha}\alpha + \frac{\bar{c}}{2V_T}\left(C_{m_q}\dot{\theta} + C_{m_{\dot{\alpha}}}\dot{\alpha}\right)\right]$$

The following relationships also hold:

$$n = \frac{C_{L_{\delta_{e=0}}} qS + F_n \sin(\alpha + i_{F_n})}{W}$$

$$\alpha = \frac{C_{L_{\delta_{e=0}}}}{C_{L_\alpha}} + \alpha_{0L}$$

$$\dot{x} = V_T \cos\gamma$$

$$\dot{h} = V_T \sin\gamma$$

6.3.2 Equations Used for Lateral Launch Studies - Canard Off

Summation of forces along the Y_b axis:

$$\dot{v} = \frac{qS}{W/g}\left[C_{y_o} + C_{y_\beta}\beta\right] + g\varphi\cos\theta - \dot{\psi}u + \dot{\phi}w$$

Summation of moments about the X_b axis:

$$\ddot{\phi} = \frac{1}{I_{x_b}}\left\{qSb\left[(C_{\ell_1} + C_{\ell_\beta}\beta) + \frac{b}{2V_T}(\dot{C}_\ell)\right] + I_{xz_b}(\ddot{\psi} + \dot{\theta}\dot{\phi}) - \dot{\theta}\dot{\psi}(I_{z_b} - I_{y_b}) - \bar{e}F_n\sin i_{F_n}\right\}$$

Summation of moments about the Z_b axis:

$$\ddot{\psi} = \frac{1}{I_{z_b}}\left\{qSb\left[(C_{n_1} + C_{n_\beta}\beta) + \frac{b}{2V_T}(\dot{C}_n)\right] + I_{xz_b}(\ddot{\phi} - \dot{\theta}\dot{\psi}) - \dot{\theta}\dot{\phi}(I_{y_b} - I_{x_b}) + \bar{e}F_n\sin i_{F_n}\right\}$$

The following relationships also hold:

$$\dot{C}_\ell = C_{\ell_p}\dot{\phi} + C_{\ell_r}\dot{\psi}$$

$$\dot{C}_n = C_{n_p}\dot{\phi} + C_{n_r}\dot{\psi}$$

$$C_{\ell_1} = C_{\ell_o} + C_{\ell_{\delta a}}\delta_a$$

$$C_{n_1} = C_{n_o} + C_{n_{\delta r}}\delta_r$$

$$u = V_T \cos \alpha$$

$$w = V_T \sin \alpha$$

$$\beta = \tan^{-1}\left(\frac{v}{V_T}\right)$$

$$\dot{y} = V_T \sin (\psi + \beta)$$

6.3.3 <u>Autopilot Equations:</u>

$$\delta_a = K_{\varphi_a} \varphi + K_{\dot{\varphi}_a} \dot{\varphi}$$

$$\delta_r = K_{\psi_r} \psi$$